Star Formation Histories of Star Forming Galaxies in a Hierarchical Universe

ChangHoon Hahn,[1, 2, 3, *] Jeremy L. Tinker,[3] and Andrew R. Wetzel[4, 5, 6]

[1] *Lawrence Berkeley National Laboratory, 1 Cyclotron Rd, Berkeley CA 94720, USA*
[2] *Berkeley Center for Cosmological Physics, University of California, Berkeley, CA 94720, USA*
[3] *Center for Cosmology and Particle Physics, Department of Physics, New York University, 4 Washington Place, New York, NY 10003*
[4] *TAPIR, California Institute of Technology, Pasadena, CA USA*
[5] *Carnegie Observatories, Pasadena, CA USA*
[6] *Department of Physics, University of California, Davis, CA USA*

ABSTRACT

We measure the timescale of star formation variability and the connection between star formation and host halo accretion histories of star-forming central galaxies. Star-forming galaxies are found to have a tight relationship between their star formation rates and stellar masses on the so-called "star-forming sequence" (SFS), which characterizes both their star formation histories and stellar mass growths. Meanwhile, observed constraints on the stellar-to-halo mass relation (SHMR) connect stellar mass growth to host halo halo accretion history. Combining these observed trends with a high-resolution cosmological N-body simulation, we present a flexible model that tracks the star formation, stellar mass, and host halo accretion histories of star-forming central galaxies over $z < 1$. We then compare this model to the observed stellar mass function and SFS of central galaxies in SDSS Data Release 7 to find that the scatter in SHMR at $M_h = 10^{12} M_\odot$, $\sigma_{\log M_*}$, is sensitive to the timescale of star formation variability, $t_{\rm duty}$. Variations on shorter timescales produce tighter $\sigma_{\log M_*}$. Stronger correlation between star formation and host halo accretion histories (higher correlation coefficient r) also produce tighter scatter in the SHMR. To reproduce $\sigma_{\log M_*}(M_h = 10^{12} M_\odot) \sim 0.2$ dex from many halo model based observational constraints and hydrodynamic simulations, we find that a correlation of $r > 0.5$ and $t_{\rm duty} \leq 1$ Gyr is necessary. For $r \sim 0.6$ constraints found in the literature, $t_{\rm duty} < 0.5$ Gyr is necessary. The lack of consensus among observations and galaxy formation model, however, remains the primary bottleneck in precisely constraining r and $t_{\rm duty}$. Nevertheless, we demonstrate that SHMR constraints can be used to constrain the timescale of star formation variability and the correlation between star formation and halo accretion history.

Keywords: methods: numerical – galaxies: evolution – galaxies: haloes – galaxies: star formation – galaxies: groups: general – cosmology: observations.

1. INTRODUCTION

Observations from large surveys such as the Sloan Digital Sky Survey (SDSS; York et al. 2000) have been critical for establishing the global trends of galaxies in the local universe. Broadly speaking, galaxies fall into two categories: quiescent and star-forming (hereafter SF) galaxies. Quiescent galaxies have little to no star formation, are red in color due to old stellar populations, and have ellipitical morphologies. Meanwhile, SF galaxies have significant star formation, thus are blue in color, and have disk-like morphologies (Kauffmann et al. 2003; Blanton et al. 2003; Baldry et al. 2006; Taylor et al. 2009; Moustakas et al. 2013; see Blanton & Moustakas 2009 and references therein). SF galaxies, furthermore, are found on the so-called "star-forming sequence" (hereafter SFS), a tight relationship between their star formation rates (SFR) and stellar masses (Noeske et al. 2007; Daddi et al. 2007; Salim et al. 2007; Speagle et al. 2014; Lee et al. 2015, see also Figure 1). This sequence, which is observed out to $z > 2$ (Wang et al. 2013; Leja et al. 2015) plays a crucial role in determining galaxy evolution over the past $\sim 10\,\mathrm{Gyr}$ (see Kelson 2014; Abramson et al. 2016, for an alternative point of view). The significant fraction of SF galaxies that quench their star formation and migrate off of the SFS reflects the growth in the fraction of quiescent galaxies (Blanton 2006; Borch et al. 2006; Bundy et al. 2006; Moustakas et al. 2013). The decline of star formation in the entire SFS (Lee et al. 2015; Schreiber et al. 2015) over time reflects the decline in overall cosmic star formation (Hopkins & Beacom 2006; Behroozi et al. 2013; Madau & Dickinson 2014). With its evolution, the SFS also connects the star formation histories of SF galaxies to their stellar mass growths.

These observations have also allowed us to investigate how galaxies fit into the context of hierarchical structure formation predicted by ΛCDM cosmology. In addition to traditional theoretical models of hydrodynamic simulations and semi-analytic models (see Silk & Mamon 2012; Somerville & Davé 2015, for reviews), empirical models halos have been remarkably successful for understanding the galaxy-halo connection. These models relate galaxy properties to their host dark matter halo properties using methods such as halo occupation distribution modeling (HOD; *e.g.* Zheng et al. 2007; Zehavi et al. 2011; Leauthaud et al. 2012; Parejko et al. 2013; Zu & Mandelbaum 2015), luminosity function modeling (*e.g.* Yang et al. 2009), and abundance matching (*e.g.* Kravtsov et al. 2004; Vale & Ostriker 2006; Conroy et al. 2009; Moster et al. 2013; Reddick et al. 2013). Using these models, we find that more massive halos host more massive galaxies with a tight scatter in the stellar-to-halo mass relation (hereafter SHMR; Mandelbaum et al. 2006; Conroy et al. 2007; More et al. 2011; Leauthaud et al. 2012; Tinker et al. 2013; Velander et al. 2014; Han et al. 2015; Zu & Mandelbaum 2015; Gu et al. 2016; Lange et al. 2018). An equally tight SHMR is found at higher $z \sim 1$ (Leauthaud et al. 2012; Tinker et al. 2013; Patel et al. 2015). This lack of evolution in the scatter of the SHMR clearly suggests that stellar mass growth of galaxies is linked somehow to the growth of their host dark matter halos.

Despite these developments, we face a number of challenges when it comes to understanding the detailed star formation histories (SFH) and its connection to host halo assembly history of galaxies. For instance, SFHs at lookback times longer than 200 Myr do not contribute to SFR indicators such

* hahn.changhoon@gmail.com

as $H\alpha$ or FUV fluxes Sparre et al. (2017). Measuring SFHs from fitting photometry or spectroscopy typically assume a specific functional form of the SFH, such as exponentially declining or lognormal, that do not include variations on short timescales (*e.g.* Wilkinson et al. 2017; Carnall et al. 2018). Even methods that recover non-parametric SFHs from high signal-to-noise observations can only retrieve SFHs in coarse temporal resolutions (*e.g.* Tojeiro et al. 2009; Leja et al. 2018). While simulations provide another means for understanding SFHs, they are also subject to their specific time and mass resolutions that suppress the variability of their star formation, especially in analytic models, semi-analytic models, and large-volume cosmological hydrodynamic simulations (Sparre et al. 2015, 2017, see also Figure **??**).

Empirical models, with its flexibility provides an effective method for examining the connection between SFH and host halo assembly history. A number of empirical models (Taghizadeh-Popp et al. 2015; Becker 2015; Rodríguez-Puebla et al. 2016; Mitra et al. 2017; Cohn 2017; Moster et al. 2017), have relate SFHs of galaxies linearly to their host halo mass accretion rates and successfully reproduce a number of observations. Such models make the strong assumption that SFH of galaxies are perfectly correlated to halo accretion history. Recent analysis of the observed correlation between the SFRs and large-scale environment of SF galaxies in Tinker et al. (2018a), however, find a correlation coefficient of only $r \sim 0.63$. These models, therefore, ignore variation in star formation independent from halo accretion, which may come from physical processes in galaxies. More recently, the empirical model of Behroozi et al. (2018) correlate SFH with halo assembly while also incorporating star formation variability in the SFH. For halos at a given $v_{\mathrm{M_{peak}}}$ (the maximum circular velocity of the halo at the redshift of max halo mass) and z, they assign higher SFRs to halos with higher values of Δv_{max} (logarithmic growth in the maximum circular velocity of the halo over past dynamical time) allowing for random scatter in the assignment. Through this random scatter, which is further separated into contributions from shorter and longer timescales, they incorporate star formation variability. Explicitly examining and constraining the timescale of star formation variability, however, is difficult with such a parameterization.

Constraints on the timescale of star formation variability can be used to shed light on physical processes involved in galaxy star formation and constrain galaxy feedback models (Sparre et al. 2015). For instance, it can be used to differentiate between physical processes such as galactic feedback interacting with the circumgalactic medium, which would cause longer timescale variations, or internal processes affecting the cold gas in the galaxy, which would cause ~ 100 Myr variations. Using the Feedback In Realistic Environments (FIRE) high resolution cosmological simulations, Hopkins et al. (2014) find that explicit and resolved feedback increases time varaibility in SFRs. Also using FIRE, Sparre et al. (2017) find that varying the strength of Type II supernova feedback can change the burstiness of SFHs. Governato et al. (2015) find that HI shielding from UV radiation and early feedback from young stars would also produce small scale star formation variability.

In this paper, we construct an empirical model of SF central galaxies, the timescale of star formation variability in their SFH, and the connection between their SFH and host halo accretion history. We focus on central galaxies since the SFHs of satellites are influenced by environmentally-driven external mechanisms such as ram pressure stripping (Gunn & Gott 1972; Bekki 2009), strangula-
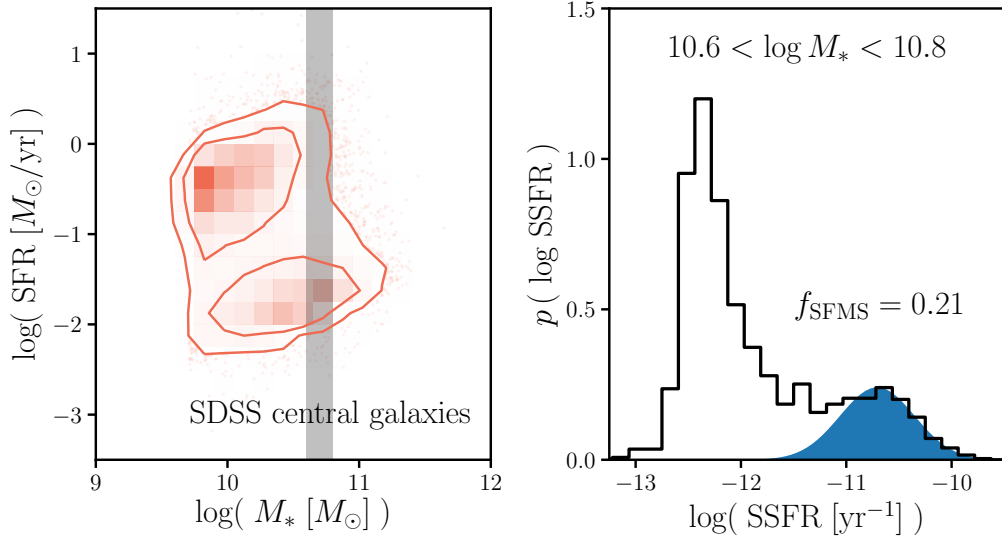
Figure 1. The SFR–M_* relation of the central galaxies in SDSS DR7 mark the bimodal distribution of the star-forming and quiescent populations (left panel). *Star-forming centrals, based on the correlation between their SFR and M_*, lie on the so-called "star-forming sequence".* On the right, we present the SSFR distribution, $p(\log \mathrm{SSFR})$, of SDSS centrals with $10.6 < \log M_* < 10.8$. Based on the SFS component from the Hahn et al. (2018b) GMM fit to the SFR–M_* relation (shaded in blue), galaxies in the SFS account for $f_{\mathrm{SFS}} = 0.21$ of the centrals in the stellar mass bin.

tion (Larson et al. 1980; Peng et al. 2015), or harassment (Moore et al. 1998). Moreover, centrals constitute the majority of massive galaxies ($M_* > 10^{9.5} M_\odot$) at $z \sim 0$ (Wetzel et al. 2013). Using a similar approach as Wetzel et al. (2013); Hahn et al. (2017a), we present a model that combines a high resolution cosmological N-body simulation with observed evolutionary trends of the SFS. Our model statistically tracks the star formation, stellar mass, and host halo assembly histories of SF central galaxies over $z \sim 1$ to 0. By comparing predictions of this empirical model to observations, in particular measurements of the scatter in the SHMR, we constrain the timescale of star formation variability and also the correlation between SFH and host halo assembly history.

In Section 2 we describe the $z \approx 0$ central galaxy sample that we construct from SDSS Data Release 7. Then in Section 3, we describe the N-body simulation and how we evolve the SFR and stellar masses of the star-forming central galaxies in our model. We compare predictions from our model to observations and present the resulting constraints in Section 4. Finally, we conclude and summarize the results in Section 5.

2. CENTRAL GALAXIES OF SDSS DR7

We construct our galaxy sample following the sample selection of Tinker et al. (2011). We select a volume-limited sample of galaxies at $z \approx 0.04$ with $M_r - 5\log(h) < -18$ and complete above $M_* > 10^{9.4} h^{-2} M_\odot$ from the NYU Value-Added Galaxy Catalog (VAGC; Blanton et al. 2005) of the Sloan Digital Sky Survey Data Release 7 (SDSS DR7; Abazajian et al. 2009). The stellar masses of these galaxies are estimated using the kcorrect code (Blanton & Roweis 2007) assuming a Chabrier

(2003) initial mass function. For their specific star formation rates (SSFR) we use measurements from the current release of the MPA-JHU spectral reductions[1] (Brinchmann et al. 2004). Generally, SSFR $> 10^{-11}\mathrm{yr}^{-1}$ are derived from Hα emission, $10^{-11} >$ SSFR $> 10^{-12}\mathrm{yr}^{-1}$ are derived from a combination of emission lines, and SSFR $< 10^{-12}\mathrm{yr}^{-1}$ are based on D_n4000 (see discussion in Wetzel et al. 2013). We emphasize that SSFR $< 10^{-12}\mathrm{yr}^{-1}$ should only be considered upper limits to the actual galaxy SSFR (Salim et al. 2007).

From this galaxy sample, we identify central galaxies using the Tinker et al. (2011) group finder, a halo-based algorithm that uses the abundance matching ansatz to iteratively assign halo masses to groups (see also Yang et al. 2005). It assigns an initial halo mass to each galaxy by matching their abundances. Then starting with the most massive galaxy, nearby lower mass galaxies are assigned a probability of being a satellite. Once all the galaxies are assigned to a group, the halo masses of the central galaxies are updated by abundance matching with the total stellar mass in the groups. This entire process is repeated until convergence. Every group contains one central galaxy, which by definition is the most massive, and a group can contain zero, one, or many satellites. As with any group finder, galaxies are misassigned due to projection effects and redshift space distortions. Our central galaxy sample has a purity of $\sim$90% and completeness of $\sim$95% (Tinker et al. 2018b) Moreover, as illustrated in Campbell et al. (2015), the Tinker et al. (2011) group finder robustly identifies red and blue centrals as a function of stellar mass, which is highly relevant to our analysis. We present the SFR–M_* relation of the SDSS DR7 central galaxies, described above, in the left panel of Figure 1. The contours of the relation clearly illustrate the bimodality in the galaxy sample with the star-forming centrals lying on the so-call "star-forming sequence" (SFS).

3. MODEL: SIMULATED CENTRAL GALAXIES

We are interesting in constructing a model that tracks central galaxies and their star formation within the heirarchical growth of their host halos. This requires a cosmological N-body simulation that accounts for the complex dynamical processes that govern the host halos of galaxies. In this paper we use the high resolution N-body simulation from Wetzel et al. (2013) generated using the White (2002) `TreePM` code with flat ΛCDM cosmology ($\Omega_m = 0.274, \Omega_b = 0.0457, h = 0.7, n = 0.95$, and $\sigma_8 = 0.8$). From initial conditions at $z = 150$, generated from second-order Lagrangian Perturbation Theory, 2048^3 particles with mass of $1.98 \times 10^8\, M_\odot$ are evolved in a $250\, h^{-1}\mathrm{Mpc}$ box with a Plummer equivalent smoothing of $2.5\, h^{-1}\mathrm{kpc}$ (Wetzel et al. 2013, 2014). 'Host halos' are then identified using the Friends-of-Friends algorithm (FoF; Davis et al. 1985) with linking length of b=0.168 times the mean inter-partcile spacing. Within these host halos, Wetzel et al. (2013) identifies 'subhalos' as overdensities in phase space through a six-dimensional FoF algorithm (FoF6D; White et al. 2010). The host halos and subhalos are then tracked across the simulation outputs from $z = 10$ to 0 to build merger trees (Wetzel et al. 2009; Wetzel & White 2010). The most massive subhalos in newly-formed host halos at a given simulation output are defined as the 'central' subhalo. A central subhalo retains its 'central' definition until it falls into a more massive host halo (FoF halo mass), at which point it becomes a 'satellite' subhalo.

---

[1] http://wwwmpa.mpa-garching.mpg.de/SDSS/DR7/

Throughout its 45 snapshot outs, `TreePM` simulation tracks the evolution of subhalos back to $z \sim 10$. We restrict ourselves to 15 snapshots from $z = 1.08$ to 0.05, where we have the most statistically meaningful observations. Furthermore, since we're interested in centrals we only keep subhalos that are classified as centrals throughout the redshift range. This criterion removes "black splash" or "ejected" satellite galaxies (*e.g.* Mamon et al. 2004; Wetzel et al. 2014) misclassified as centrals. Next, we describe how we select and initialize the SF central galaxies from the central subhalos of the `TreePM` simulation in our model.

3.1. *Selecting Star-Forming Centrals*

To construct a model that tracks the SFR and stellar mass evolution of star-forming central galaxies, we first need to select them from the central galaxies/subhalos in the `TreePM` simulation. Since we want our model to reproduce observations, our selection is based on $f_{\mathrm{SFS}}^{\mathrm{cen}}(M_*)$, the fraction of central galaxies within the SFS measured from the SDSS DR7 VAGC (Section 2). Below, we describe how we derive $f_{\mathrm{SFS}}^{\mathrm{cen}}(M_*)$ and use it to select SF central galaxies in our model. Afterwards we describe how we initialize the SFRs and M_* of these galaxies at $z = 1$.

Often in the literature, an empirical color-color or SFR–M_* cut that separates the two main modes (red/blue or star-forming/quiescent) in the distribution is chosen to classify galaxies (*e.g.* Baldry et al. 2006; Blanton & Moustakas 2009; Drory et al. 2009; Peng et al. 2010; Moustakas et al. 2013; Hahn et al. 2015). The red/quiescent or blue/star-forming fractions derived from this sort of classification, by construction, depend on the choice of cut and neglect galaxy subpopulations such as transitioning galaxies *i.e.* galaxies in the "green valley". Instead, for our $f_{\mathrm{SFS}}^{\mathrm{cen}}(M_*)$, we use the SFS identified from the Hahn et al. (2018b) method. Hahn et al. (2018b) uses Gaussian Mixture Models and the Bayesian Information Criteria in order to fit the SFR–M_* relation of a galaxy population and identify its SFS. This data-driven approach relaxes many of the assumptions and hard cuts that go into other methods. Furthermore, Hahn et al. (2018b) demonstrate its method can be flexibly applied to a wide range of SFRs and M_*s and for multiple simulations. The weight of the SFS GMM component from the method provides an estimate of $f_{\mathrm{SFS}}^{\mathrm{cen}}$. In the right panel of Figure 1, we present the SSFR distribution, $p(\log \mathrm{SSFR})$, of the SDSS DR7 central galaxies within $10.6 < \log M_* < 10.8$ with the SFS GMM component shaded in blue. The SFS constitutes $f_{\mathrm{SFS}}^{\mathrm{cen}} = 0.21$ of the SDSS central galaxies in this stellar mass bin. Using the $f_{\mathrm{SFS}}^{\mathrm{cen}}$ estimates, we fit $f_{\mathrm{SFS}}^{\mathrm{cen}}$ as a linear function of $\log M_*$ similar to Wetzel et al. (2013); Hahn et al. (2017a):

$$f_{\mathrm{SFS,bestfit}}^{\mathrm{cen}}(M_*) = -0.627 \left(\log M_* - 10.5\right) + 0.354. \tag{1}$$

We note that this is in good agreement with the $f_{\mathrm{Q}}^{\mathrm{cen}}(M_*; z \sim 0)$ fit from Hahn et al. (2017a).

To select the SF centrals from the subhalos, we begin by assigning M_* at $z \sim 0$ to the subhalos by subhalo abundance matching (SHAM) to M_{peak}, the maxmum host halo mass that it ever had as a central subhalo (Conroy et al. 2006; Vale & Ostriker 2006; Yang et al. 2009; Wetzel et al. 2012; Leja et al. 2013; Wetzel et al. 2013, 2014; Hahn et al. 2017a). SHAM, in its simplest form, assumes a one-to-one mapping between subhalo M_{peak} and galaxy stellar mass, M_*, that preserves rank order: $n(>M_{\mathrm{peak}}) > n(>M_*)$. In practice, we apply a 0.2 dex log-normal scatter in M_* at fixed M_{peak} based

on the observed SHMR (*e.g.* Mandelbaum et al. 2006; More et al. 2011; Velander et al. 2014; Zu & Mandelbaum 2015; Gu et al. 2016; Lange et al. 2018). For $n(>M_*)$, we use observed stellar mass function (SMF) from Li & White (2009), which is based on the same SDSS NYU-VAGC sample as our group catalog. Then using the SHAM M_*, we randomly select subhalos as SF based on based on the probabilities of being on the SFS using Eq. 1. Tinker et al. (2017, 2018b) found that quenching is independent of halo growth rate and therefore we randomly select SF subhalos. In our model, we assume that once a SF galaxy quenches its star formation, it remains quiescent. Without any quiescent galaxies rejuvenating their star formation, galaxies on the SFS at $z \sim 0$ are also on the SFS at $z > 0$. Using this assumption the SF centrals we select at $z \sim 0$ are also on the SFS at the intial redshift of our model: $z \sim 1$.

We next initialize the SF centrals at $z \sim 1$ using the observed SFR-M_* relation of the SFS with M_* assigned using SHAM with a $z \sim 1$ SMF interpolated between the Li & White (2009) SMF and the SMF from Marchesini et al. (2009) at $z = 1.6$. We choose the Marchesini et al. (2009) SMF, among others, because it produces interpolated SMFs that monotonically increase over $z < 1$. As noted in Hahn et al. (2017a), at $z \approx 1$, the SMF interpolated between the Li & White (2009) and Marchesini et al. (2009) SMFs is consistent with more recent measurements from Muzzin et al. (2013) and Ilbert et al. (2013). We again apply a 0.2 dex log-normal scatter in the SHAM based on observations (*e.g.* Leauthaud et al. 2012; Tinker et al. 2013; Patel et al. 2015) We next assign SFRs based on $z \sim 1$ observations in the literature. However, observations, not only use galaxy properties derived differently from the SDSS VAGC but they also find SFS with significant discrepancies from one another. Speagle et al. (2014) compiles the SFR-M_* relation of the SFS from 25 studies in the literature, each with different methods of deriving galaxy properties. Even *after* their calibration, for a fixed $M_* = 10^{10.5} M_\odot$, the SFRs of the SFSs at $z \sim 1$ vary by more than a factor of 2 (see Figure 2 of Speagle et al. 2014). With little consensus on the SFS at $z \sim 1$, and consequently its redshift evolution, we flexibly parameterize the SFS SFR, $\log \mathrm{SFR}_{\mathrm{SFS}}(M_*, z)$, with free parameters $m_{M_*}^{\mathrm{low}}$, $m_{M_*}^{\mathrm{high}}$, and m_z. These parameters characterize the stellar mass dependence of the SFS below and above $10^{10} M_\odot$ and the redshift dependence, respectively.

We parameterize the $\log \mathrm{SFR}$ of the SFS as,

$$\log \mathrm{SFR}_{\mathrm{SFS}}(M_*, z) = m_{M_*} (\log M_* - 10.) + m_z(z - 0.05) - 0.19 \tag{2}$$

$$\text{where } m_{M_*} = \begin{cases} m_{M_*}^{\mathrm{low}} & \text{for } M_* < 10^{10} M_\odot \\ m_{M_*}^{\mathrm{high}} & \text{for } M_* \geq 10^{10} M_\odot. \end{cases}$$

We assign SFRs to our SF centrals at $z \sim 1$ by sampling a log-normal distribution centered about $\log \mathrm{SFR}_{\mathrm{SFS}}(M_*, z = 1)$ with a constant scatter of 0.3 dex from observations (Daddi et al. 2007; Noeske et al. 2007; Magdis et al. 2012; Whitaker et al. 2012). Later when comparing to observations, we choose conservative priors for the parameters $m_{M_*}^{\mathrm{low}}$, $m_{M_*}^{\mathrm{high}}$ and m_z that encompass the best-fit SFS from Speagle et al. (2014) and measurements from Moustakas et al. (2013) and Lee et al. (2015). With our SF centrals initalized at $z \sim 1$, next, we describe how we evolve their SFR and M_*.
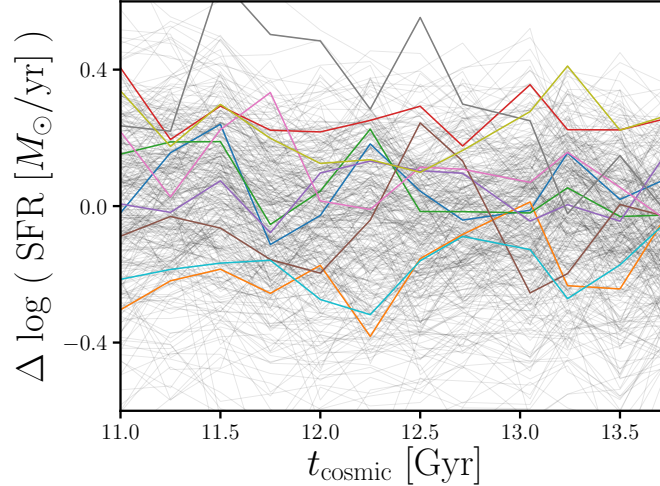
3.2. *Evolving along the Star Formation Sequence*

Figure 2. Galaxies in the Illustris simulation have SFHs that evolve along the SFS, with their SFRs stochastically fluctuating about the $\log$ SFR of the SFS. We highlight $\Delta \log$ SFR, SFR with respect to $\log$ SFR$_{\rm SFS}$ (Eq. 3), for a handful of galaxies with $10^{10.5} < M_* < 10^{10.6} M_\odot$ at $z \sim 0$. We calculate $\Delta \log$ SFR with $\log$ SFR$_{\rm SFS}$ identified using the Hahn et al. (2018b) method, same as in Section 3.1. The implementation of SFR variability in the SFHs of star-forming centrals in our model (Section 3.2) is motivated by the SFHs of Illustris galaxies above.

The tight correlation between the SFRs and stellar masses of star-forming galaxies on the SFS has been observed spanning over four orders of magnitude in stellar mass, with a roughly constant scatter of ~ 0.3 dex, and out to $z > 2$ (*e.g.* Noeske et al. 2007; Daddi et al. 2007; Elbaz et al. 2007; Salim et al. 2007; Santini et al. 2009; Karim et al. 2011; Whitaker et al. 2012; Moustakas et al. 2013; Lee et al. 2015; see also references in Speagle et al. 2014). This correlation is also predicted by modern galaxy formation models (Somerville & Davé 2015, see Hahn et al. 2018b and references therein). The SFS naturally presents itself as an anchoring relationship to characterize the star formation and M_* growth histories of SF galaxies throughout $z < 1$. More specifically, *we characterize the SFH of each star-forming central with respect to the* $\log$ SFR *of the SFS* (Eq. 2):

$$\log \text{SFR}_i(M_*, t) = \log \text{SFR}_{\rm SFS}(M_*, t) + \Delta \log \text{SFR}_i(t). \tag{3}$$

Since SFHs determine the M_* growth of galaxies, in this prescription, $\Delta \log$ SFR$_i(t)$ dictates the SFH and M_* evolution of SF central.

One simple prescription for $\Delta \log$ SFR(t) would be to keep $\Delta \log$ SFR fixed throughout $z < 1$ to the offsets from the $\log$ SFR$_{\rm SFS}$ in the initial SFRs of our SF centrals at $z \sim 1$ similar to simple analytic models such as Mitra et al. (2015). Galaxies with higher than average initial SFRs continue evolving above the average SFS, while SF centrals with lower than average initial SFRs continue evolving below the average SFS. In addition to not being able to reproduce observations, which we later demonstrate, we also do not find such SFHs in SF galaxies of hydrodynamic simulations such as Illustris (Vogelsberger et al. 2014; Genel et al. 2014). In Figure 2, we plot $\Delta \log$ SFR$_i$ of star-forming galaxies in the Illustris simulation as a function of cosmic time. These galaxies have stellar masses

Figure 3. We incorporate star formation variability in our model using a "star formation duty cycle" where the SFRs of SF centrals fluctuate about the $\log \mathrm{SFR_{SFS}}$ on some timescale t_{duty}. In our fiducial prescription, we randomly sample $\Delta \log \mathrm{SFR}$ from a log-normal distribution with 0.3 dex scatter at each timestep. We illustrate $\Delta \log \mathrm{SFR}_i(t)$ of two SF centrals with star formation duty cycles on $t_{\mathrm{duty}} = 1$ Gyr (blue) and 5 Gyr (orange) timescales in the left panel. $\Delta \log \mathrm{SFR}(t)$ determines the SFH and hence the M_* growth of the SF central galaxies (Eq. 4). On the right, we illustrate the SFR and M_* evolutions of the corresponding SF centrals. For reference, we include $\log \mathrm{SFR_{SFS}}(M_{*,i}(t), t)$ that the galaxies' SFR and M_* evolve along (black solid). We also include $\log \mathrm{SFR_{SFS}}(M_*)$ at various redshifts between $z = 1$ to 0.05 (dotted lines). *The star-forming centrals in our model evolve their SFRs and M_* along the SFS with their SFRs fluctuate about* $\log \mathrm{SFR_{SFS}}$.

within $10^{10.5}-10^{10.6} M_\odot$ at $z = 0$. At each simulation output, we calculate $\Delta \log \mathrm{SFR}_i$ using Eq. 3 with $\log \mathrm{SFR_{SFS}}$ derived from the SFS identified in the simulation using the Hahn et al. (2018b) method, same as in Section 3.1. As the highlighted $\Delta \log \mathrm{SFR}_i$ illustrate, SF galaxies in Illustris evolve along the SFS, with their SFRs fluctuating about $\log \mathrm{SFR_{SFS}}$.

Motivated by the SFHs of Illustris SF galaxies, we introduce variability to the SFHs of our SF centrals in the form of a "*star formation duty cycle*". Within the Eq. 3 SFH, we parameterize $\Delta \log \mathrm{SFR}_i$ to fluctuate about the $\log \mathrm{SFR_{SFS}}$ on timescale, t_{duty}, with amplitude sampled from a log-normal distribution with 0.3 dex scatter. For our fiducial star formation duty cycle prescription, we randomly sample $\Delta \log \mathrm{SFR}_i$ from a log-normal distribution with 0.3 dex scatter. We illustrate $\Delta \log \mathrm{SFR}_i(t)$ of SF centrals with our star formation duty cycle prescription on $t_{\mathrm{duty}} = 1$ Gyr (blue) and 5 Gyr (orange) timescales in the left panel of Figure 3. The shaded region represents the observed 0.3 dex scatter of $\log \mathrm{SFR}$ in the SFS. This $\Delta \log \mathrm{SFR}$ prescription by construction reproduces the observed log-normal SFR distribution of the SFS at any point in the model. Although, we do not expect this simplified prescription to reflect the individual SFHs of SF centrals, we seek to statistically capture the stochasticity from gas accretion, star-bursts, and feedback mechanisms for the entire SF population. Measuring t_{duty} in the duty cycle parameterization provides us with an estimate of the

timescale of such star formation variabilities and thus provide additional useful constraints on the physics of galaxy formation.

Using our fiducial SFH prescription, we evolve both the SFR and M_* of our SF centrals along the SFS. Based on Eq. 3, the SFRs of our SF centrals are functions of M_*, while M_* is the integral of the SFR over time:

$$M_*(t) = f_{\mathrm{retain}} \int_{t_0}^{t} \mathrm{SFR}(\mathrm{M}_*, \mathrm{t}') \, dt' + M_0. \tag{4}$$

t_0 and M_0 are the initial cosmic time and stellar mass at $z \sim 1$, respectively. f_{retain} here is the fraction of stellar mass that is retained after supernovae and stellar winds; we use $f_{\mathrm{retain}} = 0.6$ (Wetzel et al. 2013). We can now evolve the SFR and M_* of our SF centrals until the final $z = 0.05$ snapshot by solving the differential equation of Eqs. 3 and 4. On the right panel of Figure 3, we present the SFR and M_* evolutions of two SF centrals with $t_{\mathrm{duty}} = 1$ Gyr (blue) and 5 Gyr (orange), same as the left panel. For reference, we include the mean $\log \mathrm{SFR}$ of the SFS that the galaxies' SFR and M_* evolve along, $\log \mathrm{SFR}_{\mathrm{SFS}}(M_{*,i}(t), t)$ (black solid). We also include $\log \mathrm{SFR}_{\mathrm{SFS}}(M_*)$ (dotted lines) at various redshifts between $z = 1$ to 0.05. Based on the SFH prescription in our model, SF centrals evolve their SFRs and M_* along the SFS with their SFRs fluctuate about $\log \mathrm{SFR}_{\mathrm{SFS}}$.

3.3. Adding Assembly Bias

In our fiducial SFH prescription, we sample $\Delta \log \mathrm{SFR}_i$ randomly from a log-normal distribution with 0.3dex scatter. There is, however, growing evidence that star formation in galaxies correlate with their host halo accretion histories (*e.g.* Lim et al. 2016; Tojeiro et al. 2017; Tinker et al. 2018a). Therefore, in this section, we describe how we introduce *assembly bias* into the SFH prescription of our model. Assembly bias, most commonly in the literature, refers to the dependence of the spatial distribution of dark matter halos on halo properties besides mass (Gao et al. 2005; Wechsler et al. 2006; Gao & White 2007; Wetzel et al. 2007; Li et al. 2008; Sunayama et al. 2016). At low halo mass, older and more concentrated halos form in high density environments. While at high halo mass, the effect is the opposite — younger, less concentrated halos form in high-density regions. However, both simulations (Croton et al. 2007; Artale et al. 2018; Zehavi et al. 2018) as well as observations (Yang et al. 2006; Wang et al. 2008; Tinker et al. 2011; Wang et al. 2013; Lacerna et al. 2014; Calderon et al. 2018; Tinker et al. 2018b), CH: @JLT I'm not sure which citations you're referring to. find that this assembly bias propagates beyond spatial clustering and correlates with certain galaxy properties such as formation histories and star formation properties, an effect more specifically referred to as *galaxy* assembly bias. In our model, we incorporate galaxy assembly bias by correlating the SFHs of our SF central galaxies and their host halo accretion histories with a correlation coefficient r.

We correlate a galaxy's SFR with respect to the mean SFS SFR (*i.e.* $\Delta \log \mathrm{SFR}$ in Eq. 3) to the halo mass accretion over dynamical time. At every t_{duty} timestep, t, $\Delta \log \mathrm{SFR}(t)$ is assigned based on $\Delta M_h(t) = M_h(t) - M_h(t - t_{\mathrm{dyn}})$ in M_{max} bins with a correlation coefficient r, a parameter added to our model. This prescription for correlating $\Delta \log \mathrm{SFR}$ to ΔM_h is similar to other empirical models that also correlate $\Delta \log \mathrm{SFR}$ to ΔM_h over t_{dyn} (Rodríguez-Puebla et al. 2016; Behroozi et al. 2018). In Rodríguez-Puebla et al. (2016), however, they assume perfect ($r = 1$) correlation between SFH and
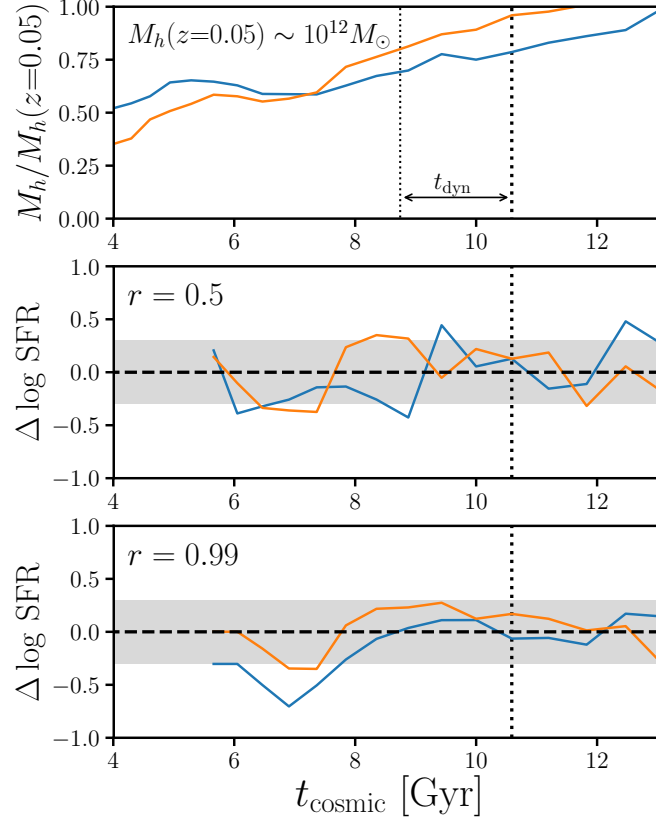
Figure 4. We incorporate assembly bias into the SF centrals of our model by correlating their host halo accretion history with their SFH with respect to the SFS. We plot the relative halo accretion history, $M_h(t)/M_h(z{=}0.05)$ for two randomly chosen SF centrals with $M_h(z{=}0.05) \sim 10^{12} M_\odot$, in the top panel. In the two panels below we present $\Delta \log \text{SFR}$, SFH with respect to the SFS, of these galaxies for our model with correlation coefficients $r = 0.5$ and 0.99 (middle and bottom). The shaded region in these panels mark the 0.3 dex 1-sigma width of the SFS. At some t (dotted), $\Delta \log \text{SFR}(t)$ is correlated with halo accretion over the period $t - t_{\rm dyn}$ to $t_{\rm dyn}$ labeled in top panel. The SFHs illustrate how $\Delta \log \text{SFR}(t)$ correlates with $\Delta M_h = M_h(t) - M_h(t - t_{\rm dyn})$ and how $\Delta \log \text{SFR}(t)$ correlates more strongly with $\Delta M_h(t)$ with higher r.

halo accretion. In the Behroozi et al. (2018) UNIVERSEMACHINE (hereafter UM), r is free parameter and their SFH includes SF variability, similar to our model. As we mention in the introduction, their prescription, however, does not not focus on a star formation variation on specific timescales as our model does through the star formation duty cycle.

In Figure 4 we illustrate this prescription for galaxy assembly bias in our model. We plot the relative halo accretion histories $M_h(t)/M_h(z{=}0.05)$ of two arbitrarily chosen SF centrals with $M_h(z{=}0.05) \sim 10^{12} M_\odot$ in the top panel (orange and blue). Below, we plot $\Delta \log \text{SFR}$, SFH with respect to the SFS, of these galaxies for our model with correlation coefficients $r = 0.5$ and 0.99 (middle and bottom). We choose a random `TreePM` snapshot, t (dotted), and label the period $[t, t - t_{\rm dyn}]$. Halo accretion over this period, $\Delta M_h = M_h(t) - M_h(t - t_{\rm dyn})$, correlates with $\Delta \log \text{SFR}(t)$.
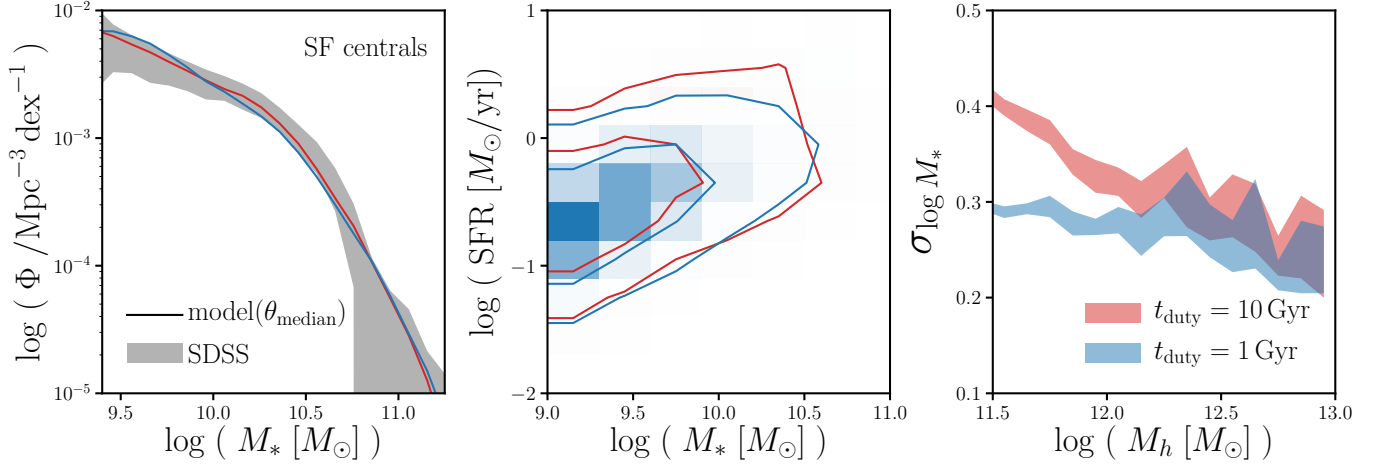
Figure 5. Our models with different star formation duty cycle timescales (blue: $t_{\rm duty}$=1 Gyr; red: $t_{\rm duty}$=10 Gyr) run with median values of their ABC posterior distribution have SMFs and SFSs consistent with observations (left and middle). *They however produce significantly different scatter in* $\log M_*$ *at fixed* $\log M_{\rm halo}$ — *scatter in the SHMR (right)*. By comparing the scatter in SHMR of our models to observational constraints on the SHMR, we constrain the timescale of the star formation duty cycle and thereby the SFHs of star forming galaxies.

The SFHs in the middle and bottom panels illustrate this correlation and how $\Delta \log {\rm SFR}(t)$ correlates more strongly with $\Delta M_h(t)$ for our model with higher r.

3.4. $\sigma_{\log M_*}$ at $z = 1$

So far in both our fiducial and assembly bias added models above, we make the assumption that the log-normal scatter in M_* at fixed M_h at $z \sim 1$, $\sigma_{\log M_*}(M_h; z = 1) = 0.2$ dex. This initial condition determines the initial SHAM M_* at $z \sim 1$ that initializes our models and is motivated by constraints on the observed SHMR (*e.g.* Leauthaud et al. 2012; Tinker et al. 2013; Patel et al. 2015). However, these $\sigma_{\log M_*}(M_h; z = 1)$ constraints are derived using halo models in which $\sigma_{\log M_*}(z = 1)$ is a constant, independent of M_h. For these models, the constraining power mainly come from massive halos. Hence, the 0.2 dex constraint does not accurately reflect $\sigma_{\log M_*}(z \sim 1)$ for less massive halos ($M_h < 10^{12} M_\odot$). Later in this paper we focus on $\sigma_{\log M_*}(M_h = 10^{12} M_\odot; z = 0)$ predicted by our models. We therefore examine the impact of varying $\sigma_{\log M_*}(z \sim 1)$ on $\sigma_{\log M_*}(M_h = 10^{12} M_\odot; z = 0)$ by introducing models with $\sigma_{\log M_*}(M_h; z = 1) = 0.35$ and 0.45 dex. Our choice is based on the $z = 1$ SHMR in the Illustris TNG (Pillepich et al. 2018) cosmological hydrodynamic simulation, which has $\sigma_{\log M_*}(z \sim 1)$ spanning 0.4 to 0.2 dex for $M_h = 10^{10.5} M_\odot$ to $10^{11.5} M_\odot$.

All of the models we present in this section track the SFRs and M_* of SF central galaxies. We can compare these properties of our model galaxies to observed galaxy population statistics (quiescent fraction and SMF) to constrain the model free parameters. Our models, run with these inferred parameters, can then be compared to observations of the galaxy-halo connection such as the SHMR. In the following section, we present this comparison and the constraints we derive on the role and timescale of star formation variability in SF central galaxies.

4. RESULTS AND DISCUSSION

Our models take `TreePM` central subhalos and tracks their SFR and M_* evolution using flexible parameterizations of the SFS and SFHs that incorporate variability through a star formation duty cycle. At $z = 0.05$, the final timestep, our models predict SFR and M_* of SF centrals, along with their host halo properties. We now use these resulting properties to compare our model to observations and constrain its free parameters — the SFS parameters of Eq. 2. Since we focus on SF centrals, the main observable we use is the SMF of SF centrals in SDSS, which we estimate as

$$\Phi_{\mathrm{SF,cen}}^{\mathrm{SDSS}} = f_{\mathrm{SFS}}^{\mathrm{cen}} \times f_{\mathrm{cen}} \times \Phi^{\mathrm{Li\&White(2009)}}. \tag{5}$$

$f_{\mathrm{SFS}}^{\mathrm{cen}}$ is the fraction of central galaxies on the SFS, which we fit in Eq. 1. f_{cen} is the central galaxy fraction from Wetzel et al. (2013) and $\Phi^{\mathrm{Li\&White(2009)}}$ is the SMF of the SDSS from Li & White (2009). If our models reproduce the observed $\Phi_{\mathrm{SF,cen}}^{\mathrm{SDSS}}$, by construction they reproduce the observed quiescent fraction.

For the comparison between our models and observation, we use the likelihood-free parameter inference framework of Approximate Bayesian Computation (ABC). ABC has the advantage over standard approaches to parameter inference in that it does not require evaluating the likelihood. For observables with likelihoods that are difficult or intractable, incorrect assumptions in the likelihood can significantly bias the posterior distributions (*e.g.* Hahn et al. 2018a). Instead, ABC relies only on a simulation of the observed data and a distance metric to quantify the "closeness" between the observed data and simulation. Many variations of ABC has been used in astronomy and cosmology (*e.g.* Cameron & Pettitt 2012; Weyant et al. 2013; Ishida et al. 2015; Alsing et al. 2018). We use ABC in conjunction with the efficient Population Monte Carlo (PMC) importance sampling as in (Hahn et al. 2017a,b). For initial sampling of our ABC particles, *i.e.* the priors of our free parameters $m_{M_*}^{\mathrm{low}}$, $m_{M_*}^{\mathrm{high}}$, and m_z, we use uniform distributions over the ranges $[0.0, 0.8]$, $[0.0, 0.8]$, and $[0.5, 2.]$, respectively. The range of the prior were conservatively chosen to encompass the best-fit SFS from Speagle et al. (2014) and measurements from Moustakas et al. (2013) and Lee et al. (2015) at $z \sim 1$. Finally, for our distance metric we use the following distance between the SMF of the star-forming centrals in our model to the observed $\Phi_{\mathrm{SF,cen}}^{\mathrm{SDSS}}$:

$$\rho_\Phi = \sum_M \left(\frac{\Phi^{\mathrm{sim}} - \Phi_{\mathrm{SF,cen}}^{\mathrm{SDSS}}}{\sigma_\Phi'} \right)^2. \tag{6}$$

$\Phi^{\mathrm{sim}}(M)$ above is the SMF of the SF centrals in our model and $\sigma_\Phi'(M)$ is the uncertainty of $\Phi_{\mathrm{SF,cen}}^{\mathrm{SDSS}}$, which we derive by scaling the Li & White (2009) uncertainty of Φ^{SDSS} derived from mock catalogs. For the rest of our ABC-PMC implementation, we strictly follow the implementation of Hahn et al. (2017b) and Hahn et al. (2017a). We refer reader to those papers for further details.

4.1. *The Fiducial Model*

We present the SMFs (left), SFSs (center), and the scatter in $\log M_*$ at M_h, $\sigma_{\log M_*}(M_h)$, (right) of our fiducial model run using SFHs with two different duty cycle timescales, $t_{\mathrm{duty}} = 10$ (red)
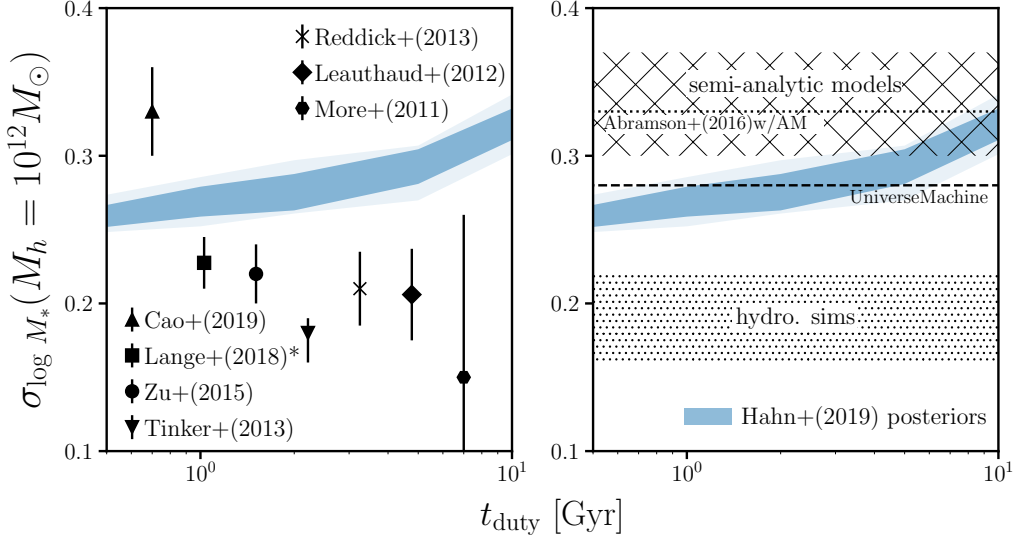
Figure 6. With shorter star formation duty cycle timescales, $t_{\rm duty}$, our model predicts smaller scatter in $\log M_*$ at $M_h = 10^{12} M_\odot$ — $\sigma_{\log M_*}$ (blue). The dark and light blue shaded regions represent the 68% and 95% confidence intervals of $\sigma_{\log M_*}$ predicted from the ABC posteriors of our model with $t_{\rm duty} = 0.5, 1, 2, 5$, and 10 Gyr. For $t_{\rm duty} = 10$ to 0.5 Gyr, $\sigma_{\log M_*}$ ranges from $0.32^{+0.019}_{-0.021}$ to $0.26^{+0.010}_{-0.012}$. In the left panel, we include for comparison observational $\sigma_{\log M_*}$ constraints from Yang et al. (2009); More et al. (2011); Leauthaud et al. (2012); Tinker et al. (2013); Zu & Mandelbaum (2015) and Cao et al. (in preparation) (see Section 4.1). We also include a constrant from Lange et al. (2018); although this constrain is on the scatter in $\log L$ at $M_h = 10^{12} M_\odot$. In the right panel, we include compiled predictions from hydrodyanmical simulations (dotted region), semi-analytic models (hatched), and the UNIVERSEMACHINE (Behroozi et al. 2018, dashed). Although there is significant tension among the observed constraints, they favor our model with star formation varability on shorter timescales. Meanwhile, even on the shortest timescales we consider, our model does not produce the low $\sigma_{\log M_*} \sim 0.2$ dex predicted by hydrodynamic simulations.

and 1 Gyr (blue), in Figure 5. For each $t_{\rm duty}$, we evaluate our fiducial model at the median parameter values of the respective posterior distributions derived using ABC. For both $t_{\rm duty}$, our model successfully produces SMFs, $\Phi^{\rm SDSS}_{\rm SF,cen}$, and SFSs consistent with observations, as expected (left and center panels). Despite their consistency with observations, however, different $t_{\rm duty}$ of the models predict i significantly different $\sigma_{\log M_*}$, particularly below $M_h < 10^{12.5} M_\odot$. We further illustrate the sensitivity of $\sigma_{\log M_*}$ of our model to $t_{\rm duty}$ in Figure 6, where we present $\sigma_{\log M_*}$ at fixed halo mass $M_h = 10^{12} M_\odot$ for our model with $t_{\rm duty} = 0.5, 1, 2, 5$, and 10 Gyr. As in Figure 5, $\sigma_{\log M_*}$ at each $t_{\rm duty}$ is predicted from our model with parameters from the corresponding ABC posterior distribution. The dark and light blue shaded regions represents the 68% and 95% confidence intervals. For $t_{\rm duty}$ ranging from 10 to 0.5 Gyr, $\sigma_{\log M_*}$ ranges from $0.32^{+0.02}_{-0.02}$ to $0.26^{+0.01}_{-0.01}$ — a shorter star formation duty cycle timescale produces significantly smaller scatter in the SHMR. *Observational constraints on the SHMR can therefore be used to constrain the timescale of star formation variability and SFH of SF central galaxies.*

On the left panel of Figure 6, we compare $\sigma_{\log M_*}$ predicted from our fiducial model to observational constraints in the literature. These constraints are mainly derived from fitting halo-occupation based models to observations of galaxy clustering, SMF, satellite kinematics, or galaxy-galaxy weak lensing. In Figure 6, we include $\sigma_{\log M_*}$ constraints from More et al. (2011); Leauthaud et al. (2012); Reddick et al. (2013); Tinker et al. (2013); Zu & Mandelbaum (2015) and Cao et al. (in preparation). More et al. (2011), Reddick et al. (2013), and Zu & Mandelbaum (2015) fit SDSS DR7 measurements of satellite kinematics, projected galaxy clustering and conditional SMF, and, galaxy clustering and galaxy-galaxy lensing, repsectively. Meanwhile, Leauthaud et al. (2012); Tinker et al. (2013) use COSMOS to fit the SMF, galaxy clustering, and galaxy-galaxy lensing. Finally, Cao et al. (in preparation) fit the kurtosis of the line-of-sight pairwise velocity dispersion between central galaxies and all neighboring galaxies to constrain the scatter in SHMR at low halo masses. We note that Leauthaud et al. (2012); Reddick et al. (2013); Zu & Mandelbaum (2015) measure $\sigma_{\log M_*}$ for all central galaxies, not only SF. Both More et al. (2011); Tinker et al. (2013), however, find a $< 1\sigma$ difference in $\sigma_{\log M_*}$ between SF and quiescent centrals, so we include these constraints in our comparison. We also include the Lange et al. (2018) constraint from fitting color-dependent conditional luminosity function and radial profile of satellite galaxies of SDSS DR7. We note that this constraint is on the scatter in luminosity, $\log L$, not $\log M_*$ at a given M_h.

Besides Cao et al. (in preparation), the $\sigma_{\log M_*}$ constraints in the literature are loosely consistent with $\sigma_{\log M_*} \sim 0.2$ dex. These constraints, however, are mostly derived using halo models that assume $\sigma_{\log M_*}$ is constant independent of M_h. The constraining power for these constraints mainly come from high mass halos and, thus, do not reflect $\sigma_{\log M_*}$ at $M_h = 10^{12} M_\odot$. While Reddick et al. (2013) constrain $\sigma_{\log M_*}$ for different bins of M_h over the range $10^{12} - 10^{14} M_\odot$, their constraints mainly come from the conditional SMF and therefore relies on the accuracy of the Tinker et al. (2011) group finder in identifying halo masses. **CH: JLT: Why does Reddick come from $10^{13} M_\odot$?** The constraint from Lange et al. (2018) is also derived from a halo model with M_h dependence. However, as mentioned above, they constrain $\sigma_{\log L}$. In More et al. (2011), where they constrain both $\sigma_{\log L}$ and $\sigma_{\log M_*}$ from the same data, they find $\sigma_{\log M_*} = 0.15^{+0.08}_{-0.11} < \sigma_{\log L} = 0.21^{+0.06}_{-0.04}$ for blue centrals. However, translating from $\sigma_{\log L}$ to $\sigma_{\log M_*}$ is tenuous for different data sets and models. We also note observational constraints include significant measurement uncertainties in M_*. The intrinsic $\sigma_{\log M_*}$ of these constraints, *i.e.* the scatter predicted by our model, will be lower. If we consider $0.1 - 0.2$ dex uncertainties in M_* (Roediger & Courteau 2015), the Cao et al. (in preparation) constraint, for instance, will be reduced from $\sigma_{\log M_*} = 0.33$ dex to $0.31 - 0.26$ dex. Overall, observational constraints favor a shorter, < 2 Gyr, duty cycle timescale for our fiducial model.

In addition to the observational constraints, we also compare the $\sigma_{\log M_*}(M_h \sim 10^{12} M_\odot)$ predicted by our model to predictions from modern galaxy formation models on the right panel: hydrodynamic simulations (dot filled), semi-analytic models (SAM; hatched), and an empirical model (dashed line). For the hydrodynamic simulations, the dotted region, $\sigma_{\log M_*} = 0.16 - 0.22$ dex, encompasses predictions from EAGLE (Matthee et al. 2017), Massive Black II (Khandai et al. 2015), and Illustris TNG, as compiled in Figure 8 of Wechsler & Tinker (2018). For the SAMs, the hatched region, $\sigma_{\log M_*} = 0.3 - 0.37$ dex, includes predictions from Lu et al. (2014); Somerville et al. (2012), and the

SAGE[2] model (Croton et al. 2016). We also include the prediction from the Behroozi et al. (2018) UM empirical model. $\sigma_{\log M_*}$ from SAMs are consistent with our model with $t_{\rm duty} \gtrsim 5$ Gyr. UM, which predicts a lower $\sigma_{\log M_*}$, is consistent with $t_{\rm duty} = 1-5$ Gyr. Lastly, hydrodynamic simulations predict the lowest $\sigma_{\log M_*}$ among the models with ~ 0.2 dex, which our fiducial model struggles to reproduce even with the shortest $t_{\rm duty}$ timescale that we consider. There is no consensus among the observational $\sigma_{\log M_*}$ constraints at $M_h \sim 10^{12} M_\odot$. However, at $M_h > 10^{12} M_\odot$ observations are in better agreement and *only* hydrodynamic simulations predict $\sigma_{\log M_*}$ low enough to be consistent (Wechsler & Tinker 2018). To reproduce observational constraints and predictions from hydrodynamic simulations, SF central galaxies in our fiducial model require star formation varability on short timescales, $\lesssim 1$ Gyr.

A key element of our models is the SFH prescription for SF central galaxies where the SFH evolves about the SFS. Contrary to our SFH prescription, Kelson (2014), for example, argue that the SFS is a consequence of central limit theorem and can be reproduced even if *in situ* stellar mass growth is modeled as a stochastic process like a random walk. Gladders et al. (2013); Abramson et al. (2015, 2016), similarly argue that ~ 2000 loosely constrained log-normal SFHs can reproduce observations such as the SMF at $z \leq 8$ and the SFS at $z \leq 6$. These works, however, focus on reproducing observations of galaxy properties and do not examine the galaxy-halo connection such as the SHMR. In order to test whether log-normal SFHs can also produce realistic SHMRs, we construct a simple empirical model using the SFHs, $\mathrm{SFR}(t)$ and $M_*(t)$, from Abramson et al. (2016) and assign them to halos by abundance matching their M_* to M_h at $z{\sim}1$. We then restrict the SFHs to those that would be classified as star-forming based on a log $\mathrm{SSFR} > -11$. cut. Afterwards we measure $\sigma_{\log M_*}$ at the lowest M_h where it can be reliably measured given the Abramson et al. (2016) sample's $M_* > 10^{10} M_\odot$ limit. We find that the Abramson et al. (2016) based empirical model predicts a scatter of $\sigma_{\log M_*}(M_h = 10^{12.4}) = 0.33 \pm 0.04$ (dotted; right panel of Figure 6). Although the Abramson et al. (2016) SFHs can reproduce a number of galaxy observations, without star formation varability on short timescales the empirical model struggles to produce $\sigma_{\log M_*}$ comparable to observational constraints and predictions from UM and hydrodynamic simulations.

The Abramson et al. (2016) based empirical model that we explore utilizes a simple abundance matching scheme. Diemer et al. (2017) find that their their log-normal fits to the SFHs of Illustris galaxies correlate with halo formation histories. Incorporating such correlations into the abundance matching may reduce $\sigma_{\log M_*}$. In fact, although we demonstrate in this section that star formation variability in the SFH on short timescales significantly reduces $\sigma_{\log M_*}(M_h = 10^{12})$, this alone is insufficient to produce the tight scatter in SHMR found in observations and hydrodynamic simulations. In the next section, we explore how correlation between SFH and halo formation histories impacts $\sigma_{\log M_*}(M_h = 10^{12})$ using our models with assembly bias.

4.2.   *Models with Assembly Bias: $r > 0$*

A shorter star formation duty cycle timescale produces tighter scatter in the SHMR of our fiducial model. This dependence on the duty cycle timescale, allows us to compare the model with measurements of $\sigma_{\log M_*}$ and predictions from galaxy formation models to constrain $t_{\rm duty}$, which reflect
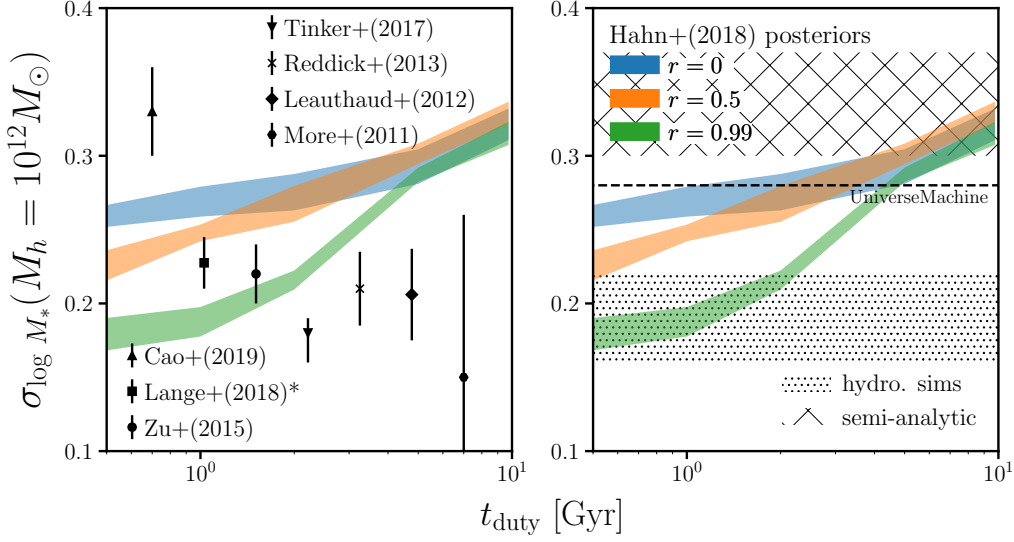

Figure 7. When we incorporate assembly bias, $\sigma_{\log M_*}$ of our model flexibly spans the various observational constraints and predictions from galaxy formation models. We plot $\sigma_{\log M_*}(M_h = 10^{12} M_\odot)$ as a function of the star formation duty cycle timescale, $t_{\rm duty}$, for our best-fit model with no assembly bias (blue) and with correlation coefficients between host halo accretion history and SFH of $r = 0.5$ (orange) and 0.99 (green). Stronger assembly bias at $t_{\rm duty} < 5\,{\rm Gyr}$ significantly reduces the scatter in SHMR, $\sigma_{\log M_*}$. In the left and right panels, we include observational cosntraints and predictions from galaxy formation models from Figure 6. We also include on the right $\sigma_{\log M_*}$ derived from matching Abramson et al. (2016) SFHs to halos via abundance matching. Strong assembly bias $r > 0.5$ and $t_{\rm duty} < 1\,{\rm Gyr}$ are necessary to produce the tight scatter in SHMR ($\sigma_{\log M_*} \sim 0.2$ dex) found in some of the observational cosntraints and predicted by hydrodynamic simulations.

the star formation variability timescale. Such comparisons in the previous section, demonstrate that $t_{\rm duty} \lesssim 2\,{\rm Gyr}$ is favored by observational constraints. However, a short duty cycle timescale alone is not enough to conservatively reproduce the $\sigma_{\log M_*}$ constraints from some obsevations and predicted by hydrodynamic simulations. Therefore, in this section, we examine how assembly bias impacts $\sigma_{\log M_*}$ using our models that correlate SFH with host halo accretion history ($r > 0$).

We repeat our analysis of inferring model parameters by comparing to observations using ABC-PMC — this time for our model with galaxy assembly bias over a grid of $t_{\rm duty}$ and r values. Using the resulting posterior distributions, we examine the scatter in the SHMR ($\sigma_{\log M_*}$) predicted by our model as a function of $t_{\rm duty}$ with $r = 0$ (no assembly bias; blue), 0.5 (orange), and 0.99 (green) in Figure 7. The shaded regions represent the 68% confidence interval of the predicted $\sigma_{\log M_*}$. We again emphasize that for all sets of ($t_{\rm duty}$, r) our models reproduce the observed SMF of SF centrals and SFS. At $t_{\rm duty} \geq 5\,{\rm Gyr}$ we find no significant difference in $\sigma_{\log M_*}$, regardless of r. Below $t_{\rm duty} < 5\,{\rm Gyr}$, however, $\sigma_{\log M_*}$ of our model decreases significantly as the SFH of SF galaxies are more correlated with halo accretion history. For $t_{\rm duty} = 0.5\,{\rm Gyr}$, we find $\sigma_{\log M_*} = 0.26^{+0.01}_{-0.01}, 0.22^{+0.01}_{-0.01}$, and $0.17^{+0.01}_{-0.02}$ for $r = 0.0, 0.5$, and 0.99, respectively.

Comparing our $r > 0$ models to the observational constraints in Figure 6, we find that assembly bias significantly reduces the tensions with observations (left panel of Figure 7). With a short star formation duty cycle ($t_{\rm duty} \leq 1\,{\rm Gyr}$) and galaxy assembly bias with $r \geq 0.5$, our model is in agreement with these $\sigma_{\log M_*} \sim 0.2$ dex constraints. On the other hand, assembly bias increases the tension with Cao et al. (in preparation), which specifically constrains $\sigma_{\log M_*}$ for $M_h \sim 10^{12} M_\odot$. We also compare our $r > 0$ models to predictions from galaxy formation models on the right panel. By varying r and $t_{\rm duty}$, $\sigma_{\log M_*}$ of our model can reproduce all of the model predictions. Focusing on hydrodynamic simulations, which best reproduce $\sigma_{\log M_*}$ observations at high M_h, we find that with a short duty cycle timescale, $t_{\rm duty} < 1$ Gyr, and $r > 0.5$ our models produces the predicted tight scatter in SHMR. We also note that with a short $t_{\rm duty}$ and high r, our models can produce $\sigma_{\log M_*}$ at $z = 0$ that have lower than the input $\sigma_{\log M_*} = 0.2$ dex at $z = 1$.

A shorter $t_{\rm duty}$ or higher r both produce smaller $\sigma_{\log M_*}$ (Figure 7). We highlight this degeneracy in Figure 8, where we plot $\sigma_{\log M_*}$ (contour and color map) as a function of $t_{\rm duty}$ and r. Regardless of the degeneracy, to produce $\sigma_{\log M_*} \sim 0.2$ dex both $t_{\rm duty} \leq 1$ Gyr and $r > 0.5$. In the literature, Tinker et al. (2018a) find correlation between $\dot{M}_h$ and log SSFR with $r = 0.63$ (dashed) and Behroozi et al. (2018) similarly find a correlation between SFH and halo assembly history with $r_c \sim 0.6$ for halos with $M_h \sim 10^{12} M_\odot$ (dotted). Using these r constraints, we find that SF variability on timescales < 0.5 Gyr is necessary to produce $\sigma_{\log M_*} \sim 0.2$ dex as found in More et al. (2011); Leauthaud et al. (2012); Reddick et al. (2013); Tinker et al. (2013); Zu & Mandelbaum (2015) and hydrodynamic simulations. We note that this timescale is shorter than the timescale ~ 0.5 Gyr that Sparre et al. (2015) find in Illustris galaxies using a Principal Component Analysis of the SFHs. However, it is consistent with the shorter ~ 0.1 Gyr timescales found in the FIRE simulations (Hopkins et al. 2014; Sparre et al. 2017).

In this section, we use our $r > 0$ models to find that correlation between SFH and halo assembly history reduces the predicted $\sigma_{\log M_*}$. With assembly bias added, our models can flexibly produce $\sigma_{\log M_*}$ constraints from observations and modern galaxy formation models over $0.2 - 0.35$ dex. To reproduce $\sigma_{\log M_*} \sim 0.2$ dex from observations and hydrodynamic simulations both $t_{\rm duty} \leq 1$ Gyr and $r > 0.5$. If we take the $r \sim 0.6$ constraints from the literature, $t_{\rm duty} < 0.5$ Gyr is necessary. This, however, is based on the 0.2 dex constraint, which for observations are derived from halo models where constraining power come from the most massive halos (Section 4.1). The Cao et al. (in preparation) constraint is the only one which specifically measures $\sigma_{\log M_*}$ at $M_h \sim 10^{12} M_\odot$ and they find significantly higher scatter. Though hydrodynamic simulations consistently find $\sigma_{\log M_*}$ at $M_h = 10^{12} M_\odot$, right below this M_h they predict significantly higher scatter — $\sigma_{\log M_*}(M_h \sim 10^{11.5}) = 0.22 - 0.32$ dex (Wechsler & Tinker 2018). Relaxing the $\sigma_{\log M_*} \sim 0.2$ constraint relaxes our constraints on $t_{\rm duty}$ to < 5 Gyr. Similar to the $\sigma_{\log M_*}$ constraint at $z = 0$, $\sigma_{\log M_*}(z \sim 1) = 0.2$ dex, which we use to initialize M_* at $z \sim 1$, is also based on halo model observational constraints. Next, we explore models with $\sigma_{\log M_*}(z \sim 1) > 0.2$ and their predictions for the scatter in SHMR at $z = 0$.

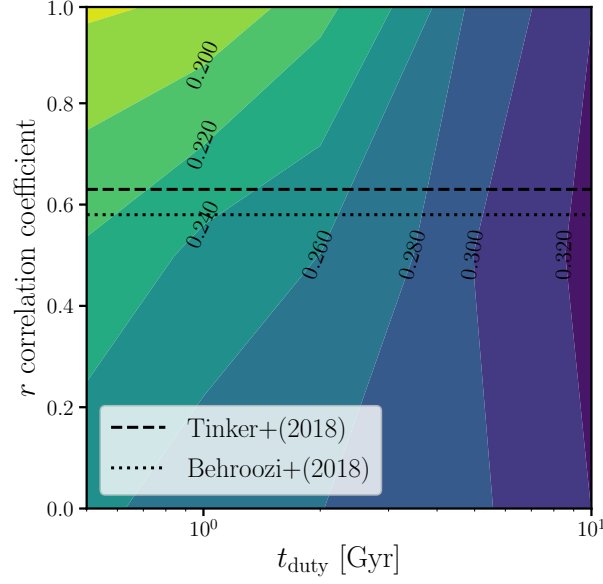### 4.3. *Models with $\sigma_{\log M_*}(z \sim 1) > 0.2$ dex*

Figure 8. $\sigma_{\log M_*}$ predicted by our model as a function of t_{duty} and r illustrates the degeneracy between the timescale of SF variability and the correlation between SFH and halo assembly history. We plot constraints on the correlation coefficient, r, from previous works in the literature: Tinker et al. (2018a) (dashed) and Behroozi et al. (2018) (dotted). Using these r constraints, to produce $\sigma_{\log M_*} \sim 0.2$ dex found in More et al. (2011); Leauthaud et al. (2012); Reddick et al. (2013); Tinker et al. (2013); Zu & Mandelbaum (2015) and hydrodynamic simulations, SF variability on timescales < 0.5 Gyr is necessary. The $\sigma_{\log M_*}$ constraint of Cao et al. (in preparation) and predictions from SAMs and UNIVERSEMACHINE, however, requires a less stringent restriction, $t_{\mathrm{duty}} < 5$ Gyr.
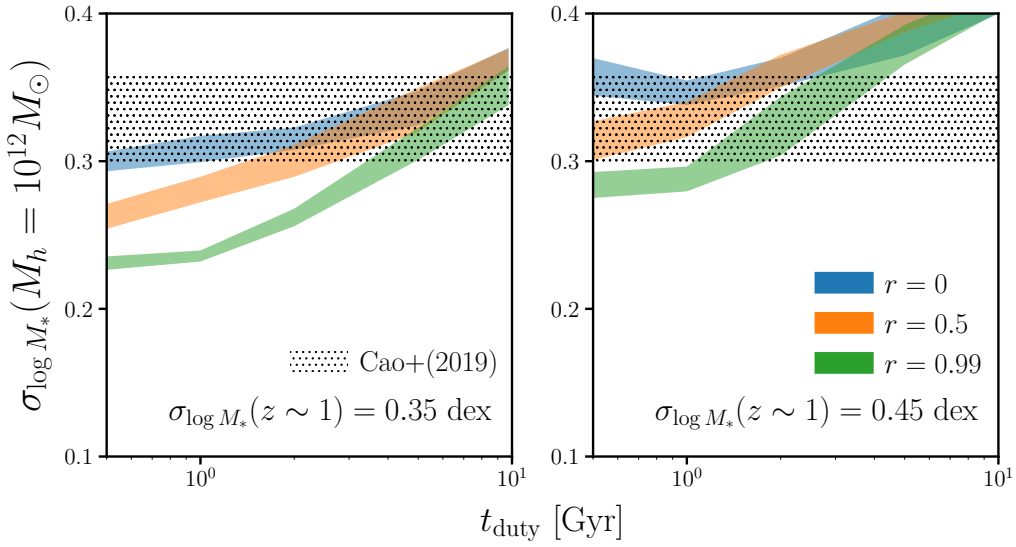
Figure 9.

The SHMR scatter at $z \sim 1$, $\sigma_{\log M_*}(z \sim 1) = 0.2$ dex, we use to determine the initial SHAM M_* at $z \sim 1$ (Section 3.1) is based on observations (*e.g.* Leauthaud et al. 2012; Tinker et al. 2013; Patel et al. 2015). However, these $z \sim 1$ constraints are derived from some halo model where much of the constraining power come from massive halos. Hence, the 0.2 dex does not *necessarily* reflect $\sigma_{\log M_*}(z \sim 1)$ at low $M_h < 10^{12} M_\odot$. We therefore use models with $\sigma_{\log M_*}(z \sim 1) > 0.2$ dex and examine their predicted $\sigma_{\log M_*}(M_h = 10^{12} M_\odot; z = 0)$. Motivated by the $z = 1$ SHMR in the Illustris TNG, which has $\sigma_{\log M_*}(z \sim 1)$ spanning 0.4 to 0.2 dex for $M_h = 10^{10.5} M_\odot$ to $10^{11.5} M_\odot$, we repeat our analysis using models with $\sigma_{\log M_*}(z \sim 1) = 0.35$ and 0.45 dex and $r = 0$, 0.5, and 0.99.

We present the $\sigma_{\log M_*}(M_h = 10^{12} M_\odot; z = 0)$ predictions made by these models as a function of $t_{\rm duty}$ in Figure 9. Increasing $\sigma_{\log M_*}(z \sim 1)$ to 0.35 and 0.45 dex significantly increases $\sigma_{\log M_*}(M_h = 10^{12} M_\odot; z = 0)$ for all $t_{\rm duty}$ and r. With $\sigma_{\log M_*}(z \sim 1) > 0.2$ dex, our models can reproduce the Cao et al. (in preparation) $\sigma_{\log M_*} \sim 0.3$ dex constraint (dotted) and predictions from SAMs for a broad range of r and $t_{\rm duty}$ values. Meanwhile, our $\sigma_{\log M_*}(z \sim 1) > 0.2$ dex models even with $t_{\rm duty} = 0.5$ Gyr and $r = 0.99$ struggle to reproduce the 0.2 dex constraints from More et al. (2011); Leauthaud et al. (2012); Reddick et al. (2013); Tinker et al. (2013); Zu & Mandelbaum (2015) and hydrodynamical simulations. Figure 9 also demonstrate that regardless of $\sigma_{\log M_*}(z \sim 1)$ a shorter duty cycle timescale and stronger assembly bias produce tighter $\sigma_{\log M_*}(z \sim 0)$. In our $\sigma_{\log M_*}(z \sim 1) > 0.2$ dex models, a short $t_{\rm duty}$ alone can significantly decrease the scatter in the SHMR from $z = 1$ to 0. For $t_{\rm duty} = 0.5$ Gyr $\sigma_{\log M_*}$ decreases by 0.5 dex. With $t_{\rm duty} = 0.5$ Gyr and $r > 0.5$, $\sigma_{\log M_*}$ decreases by 1 dex.

Throughout this section, we use our models with different $t_{\rm duty}$, r, and $\sigma_{\log M_*}(z \sim 1)$ to explore how these parameters impact $\sigma_{\log M_*}(M_h \sim 10^{12} M_\odot)$ at $z = 0$. A shorter timescale of star formation variation, $t_{\rm duty}$, produces a tighter scatter in SHMR. Similarly, higher correlation between SFH and halo assembly history also produces a tighter scatter in SHMR. Furthermore, this $t_{\rm duty}$ and r dependnece is independent of $\sigma_{\log M_*}(z \sim 1)$. The response of $\sigma_{\log M_*}(M_h \sim 10^{12} M_\odot; z = 0)$ to changes in $t_{\rm duty}$ and r illustrate the potential for the SHMR relation and it scatters in better understanding the SFH and assembly bias of SF central galaxies. The main obstacle is the lack of consensus among observations as well as simulations in the scatter of SHMR both at $z = 0$ and 1. A better consensus among observations will enable better constraints on $t_{\rm duty}$. Upcoming surveys such as the Bright Galaxy Survey of the Dark Energy Spectroscopic Instrument (DESI; Collaboration et al. 2016), which will observe $\sim$10 million galaxies down to the magnitude limit $r \sim 20$, will allow the most precise constraints of $\sigma_{\log M_*}$ at $z \sim 0$. The Galaxy Evolution Survey of the Prime Focus Spectrograph (PFS; ?), which will observe $\sim 400,000$ galaxies between $0.5 < z < 2.$ and will allow precise constraints of $\sigma_{\log M_*}$ at $z \sim 1$.

5. SUMMARY AND CONCLUSION

Despite our progress in understanding how galaxies form and evolve in the ΛCDM hierarchical universe, our understanding of the detailed star formation histories of galaxies and their connection to host halo assembly histories have been limited. This is in part due to the challenges in directly measuring SFHs in both observations and galaxy formation models. Empirical models, with their flexible prescriptions have made significant progress in better quantifying the SFHs of galaxies. These models, however, have yet to examine and constrain the timescale of star formation variability, which

has the potential to constrain physical processes involved in star formation and galaxy feedback models. In this paper, we therefore focus on measuring the timescale timescale of star formation variability and the connection between star formation and host halo accretion histories of star-forming central galaxies.

We combine the high-resolution cosmological N-body `TreePM` simulation with SFHs that evolve the SF central galaxies along the SFS and present a model that tracks the SFR, M_*, and host halo accretion histories of SF centrals from $z \sim 1$ to $z = 0.05$. More specifically, we characterize the SFHs to evolve with respect to the mean log SFR of the SFS with a "star formation duty cycle" that introduces star formation variability on some specific timescale, $t_{\rm duty}$. We parameterize the SFS using parameters that dictate the low M_* and high M_* slopes and redshift evolution. We then compare this model to the observed SMF of the SF centrals in the SDSS DR7 group catalog using ABC-PMC likelihood-free parameter inference framework. When we examine the SHMR predicted by the model and inferred parameters we find:

- A shorter star formation duty cycle in our model produces significantly tighter scatter in the SHMR at $M_h = 10^{12} M_\odot$. For $t_{\rm duty}$ from 10 to 0.5 Gyr, our model predicts $\sigma_{\log M_*}(M_h = 10^{12} M_\odot)$=$0.32^{+0.019}_{-0.021}$ to $0.26^{+0.010}_{-0.012}$. The dependence of $\sigma_{\log M_*}$ on $t_{\rm duty}$ demonstrates that the scatter in SHMR can be used to constrain $t_{\rm duty}$, which represents the timescale of star formation variability.

- We compare the $\sigma_{\log M_*}(M_h \sim 10^{12} M_\odot)$ predicted by our model to observed constraints from halo occupation modeling of galaxy clustering, SMF, satellite kinematics, and galaxy-galaxy weak lensing. Although there is tension among the constraints, comparison to observations generally favor a shorter timescale with $t_{\rm duty} \lesssim 2$ Gyr. There is also tension among prediction from galaxy formation models. To produce the $\sigma_{\log M_*} \sim 0.2$ dex predicted in hydrodynamic simulations, which best reproduce the observed $\sigma_{\log M_*}$ at $M_h > 10^{12} M_\odot$, variations on $t_{\rm duty} \lesssim 0.5$ Gyr are necessary.

- We next incorporate assembly bias in our model by correlating the star formation histories to host halo accretion histories with correlation coefficient, r. With stronger correlation, higher r, our model predict tighter scatter in the SHMR down to $\sigma_{\log M_*}(M_h = 10^{12} M_\odot)$=0.17. For $\sigma_{\log M_*}(M_h = 10^{12} M_\odot) \sim 0.2$ dex, both $r > 0.5$ and $t_{\rm duty} < 1$ Gyr are necssary; for correlation of $r \sim 0.6$ found in the literature, $t_{\rm duty} < 0.5$ Gyr is necssary.

Our work demonstrates that constraints on the scatter in the SHMR can be used to constrain both the timescale of star formation variability and the correlation between SFH and halo accretion history. The main bottleneck in deriving precise constraints on the timescale of star formation variability remains the lack of consensus among $\sigma_{\log M_*}(M_h = 10^{12} M_\odot)$ observations, which currently span 0.18 dex. Upcoming surveys, such as the DESI BGS, will have the capability to more precisely constrain $\sigma_{\log M_*}$ and resolve current tensions in observations. With such measurements, our model will be able to constrain $t_{\rm duty}$ and the physical processes that dictate star formation in galaxies.

REFERENCES

Abazajian, K. N., Adelman-McCarthy, J. K., Agüeros, M. A., et al. 2009, The Astrophysical Journal Supplement Series, 182, 543, doi: 10.1088/0067-0049/182/2/543

Abramson, L. E., Gladders, M. D., Dressler, A., et al. 2016, The Astrophysical Journal, 832, 7, doi: 10.3847/0004-637X/832/1/7

—. 2015, The Astrophysical Journal Letters, 801, L12, doi: 10.1088/2041-8205/801/1/L12

Alsing, J., Wandelt, B., & Feeney, S. 2018, arXiv:1801.01497 [astro-ph]. https://arxiv.org/abs/1801.01497

Artale, M. C., Zehavi, I., Contreras, S., & Norberg, P. 2018, Monthly Notices of the Royal Astronomical Society, 480, 3978, doi: 10.1093/mnras/sty2110

Baldry, I. K., Balogh, M. L., Bower, R. G., et al. 2006, Monthly Notices of the Royal Astronomical Society, 373, 469, doi: 10.1111/j.1365-2966.2006.11081.x

Becker, M. R. 2015, arXiv e-prints, 1507, arXiv:1507.03605

Behroozi, P., Wechsler, R., Hearin, A., & Conroy, C. 2018, ArXiv e-prints, 1806, arXiv:1806.07893

Behroozi, P. S., Wechsler, R. H., & Conroy, C. 2013, The Astrophysical Journal, 770, 57, doi: 10.1088/0004-637X/770/1/57

Bekki, K. 2009, Monthly Notices of the Royal Astronomical Society, 399, 2221, doi: 10.1111/j.1365-2966.2009.15431.x

Blanton, M. R. 2006, The Astrophysical Journal, 648, 268, doi: 10.1086/505628

Blanton, M. R., & Moustakas, J. 2009, Annual Review of Astronomy and Astrophysics, 47, 159, doi: 10.1146/annurev-astro-082708-101734

Blanton, M. R., & Roweis, S. 2007, The Astronomical Journal, 133, 734, doi: 10.1086/510127

Blanton, M. R., Hogg, D. W., Bahcall, N. A., et al. 2003, The Astrophysical Journal, 594, 186, doi: 10.1086/375528

Blanton, M. R., Schlegel, D. J., Strauss, M. A., et al. 2005, The Astronomical Journal, 129, 2562, doi: 10.1086/429803

Borch, A., Meisenheimer, K., Bell, E. F., et al. 2006, Astronomy and Astrophysics, 453, 869, doi: 10.1051/0004-6361:20054376

Brinchmann, J., Charlot, S., White, S. D. M., et al. 2004, Monthly Notices of the Royal Astronomical Society, 351, 1151, doi: 10.1111/j.1365-2966.2004.07881.x

Bundy, K., Ellis, R. S., Conselice, C. J., et al. 2006, The Astrophysical Journal, 651, 120, doi: 10.1086/507456

Calderon, V. F., Berlind, A. A., & Sinha, M. 2018, Monthly Notices of the Royal Astronomical Society, 480, 2031, doi: 10.1093/mnras/sty2000

Cameron, E., & Pettitt, A. N. 2012, Monthly Notices of the Royal Astronomical Society, 425, 44, doi: 10.1111/j.1365-2966.2012.21371.x

Campbell, D., van den Bosch, F. C., Hearin, A., et al. 2015, Monthly Notices of the Royal Astronomical Society, 452, 444, doi: 10.1093/mnras/stv1091

Carnall, A. C., Leja, J., Johnson, B. D., et al. 2018, arXiv:1811.03635 [astro-ph]. https://arxiv.org/abs/1811.03635

Chabrier, G. 2003, Publications of the Astronomical Society of the Pacific, 115, 763, doi: 10.1086/376392

Cohn, J. D. 2017, Monthly Notices of the Royal Astronomical Society, 466, 2718, doi: 10.1093/mnras/stw3202

Collaboration, D., Aghamousa, A., Aguilar, J., et al. 2016, arXiv:1611.00036 [astro-ph]. https://arxiv.org/abs/1611.00036

Conroy, C., Gunn, J. E., & White, M. 2009, The Astrophysical Journal, 699, 486, doi: 10.1088/0004-637X/699/1/486

Conroy, C., Wechsler, R. H., & Kravtsov, A. V. 2006, The Astrophysical Journal, 647, 201, doi: 10.1086/503602

Conroy, C., Prada, F., Newman, J. A., et al. 2007, The Astrophysical Journal, 654, 153, doi: 10.1086/509632

Croton, D. J., Gao, L., & White, S. D. M. 2007, Monthly Notices of the Royal Astronomical Society, 374, 1303, doi: 10.1111/j.1365-2966.2006.11230.x

Croton, D. J., Stevens, A. R. H., Tonini, C., et al. 2016, The Astrophysical Journal Supplement Series, 222, 22, doi: 10.3847/0067-0049/222/2/22

Daddi, E., Dickinson, M., Morrison, G., et al. 2007, The Astrophysical Journal, 670, 156, doi: 10.1086/521818

Davis, M., Efstathiou, G., Frenk, C. S., & White, S. D. M. 1985, The Astrophysical Journal, 292, 371, doi: 10.1086/163168

Diemer, B., Sparre, M., Abramson, L. E., & Torrey, P. 2017, The Astrophysical Journal, 839, 26, doi: 10.3847/1538-4357/aa68e5

Drory, N., Bundy, K., Leauthaud, A., et al. 2009, The Astrophysical Journal, 707, 1595, doi: 10.1088/0004-637X/707/2/1595

Elbaz, D., Daddi, E., Le Borgne, D., et al. 2007, Astronomy and Astrophysics, 468, 33, doi: 10.1051/0004-6361:20077525

Gao, L., Springel, V., & White, S. D. M. 2005, Monthly Notices of the Royal Astronomical Society, 363, L66, doi: 10.1111/j.1745-3933.2005.00084.x

Gao, L., & White, S. D. M. 2007, Monthly Notices of the Royal Astronomical Society, 377, L5, doi: 10.1111/j.1745-3933.2007.00292.x

Genel, S., Vogelsberger, M., Springel, V., et al. 2014, Monthly Notices of the Royal Astronomical Society, 445, 175, doi: 10.1093/mnras/stu1654

Gladders, M. D., Oemler, A., Dressler, A., et al. 2013, The Astrophysical Journal, 770, 64, doi: 10.1088/0004-637X/770/1/64

Governato, F., Weisz, D., Pontzen, A., et al. 2015, Monthly Notices of the Royal Astronomical Society, 448, 792, doi: 10.1093/mnras/stu2720

Gu, M., Conroy, C., & Behroozi, P. 2016, The Astrophysical Journal, 833, 2, doi: 10.3847/0004-637X/833/1/2

Gunn, J. E., & Gott, III, J. R. 1972, The Astrophysical Journal, 176, 1, doi: 10.1086/151605

Hahn, C., Beutler, F., Sinha, M., et al. 2018a, ArXiv e-prints, 1803, arXiv:1803.06348

Hahn, C., Tinker, J. L., & Wetzel, A. R. 2017a, The Astrophysical Journal, 841, 6, doi: 10.3847/1538-4357/aa6d6b

Hahn, C., Vakili, M., Walsh, K., et al. 2017b, Monthly Notices of the Royal Astronomical Society, 469, 2791, doi: 10.1093/mnras/stx894

Hahn, C., Blanton, M. R., Moustakas, J., et al. 2015, The Astrophysical Journal, 806, 162, doi: 10.1088/0004-637X/806/2/162

Hahn, C., Starkenburg, T. K., Choi, E., et al. 2018b

Han, J., Eke, V. R., Frenk, C. S., et al. 2015, Monthly Notices of the Royal Astronomical Society, 446, 1356, doi: 10.1093/mnras/stu2178

Hopkins, A. M., & Beacom, J. F. 2006, The Astrophysical Journal, 651, 142, doi: 10.1086/506610

Hopkins, P. F., Kereš, D., Oñorbe, J., et al. 2014, Monthly Notices of the Royal Astronomical Society, 445, 581, doi: 10.1093/mnras/stu1738

Ilbert, O., McCracken, H. J., Le Fèvre, O., et al. 2013, Astronomy and Astrophysics, 556, A55, doi: 10.1051/0004-6361/201321100

Ishida, E. E. O., Vitenti, S. D. P., Penna-Lima, M., et al. 2015, Astronomy and Computing, 13, 1, doi: 10.1016/j.ascom.2015.09.001

Karim, A., Schinnerer, E., Martínez-Sansigre, A., et al. 2011, The Astrophysical Journal, 730, 61, doi: 10.1088/0004-637X/730/2/61

Kauffmann, G., Heckman, T. M., White, S. D. M., et al. 2003, Monthly Notices of the Royal Astronomical Society, 341, 54, doi: 10.1046/j.1365-8711.2003.06292.x

Kelson, D. D. 2014, arXiv:1406.5191 [astro-ph]. https://arxiv.org/abs/1406.5191

Khandai, N., Di Matteo, T., Croft, R., et al. 2015, Monthly Notices of the Royal Astronomical Society, 450, 1349, doi: 10.1093/mnras/stv627

Kravtsov, A. V., Berlind, A. A., Wechsler, R. H., et al. 2004, The Astrophysical Journal, 609, 35, doi: 10.1086/420959

Lacerna, I., Padilla, N., & Stasyszyn, F. 2014, Monthly Notices of the Royal Astronomical Society, 443, 3107, doi: 10.1093/mnras/stu1318

Lange, J. U., van den Bosch, F. C., Zentner, A. R., Wang, K., & Villarreal, A. S. 2018, arXiv:1811.03596 [astro-ph]. https://arxiv.org/abs/1811.03596

Larson, R. B., Tinsley, B. M., & Caldwell, C. N. 1980, The Astrophysical Journal, 237, 692, doi: 10.1086/157917

Leauthaud, A., Tinker, J., Bundy, K., et al. 2012, The Astrophysical Journal, 744, 159, doi: 10.1088/0004-637X/744/2/159

Lee, N., Sanders, D. B., Casey, C. M., et al. 2015, The Astrophysical Journal, 801, 80, doi: 10.1088/0004-637X/801/2/80

Leja, J., Carnall, A. C., Johnson, B. D., Conroy, C., & Speagle, J. S. 2018, arXiv:1811.03637 [astro-ph]. https://arxiv.org/abs/1811.03637

Leja, J., van Dokkum, P., & Franx, M. 2013, The Astrophysical Journal, 766, doi: 10.1088/0004-637X/766/1/33

Leja, J., van Dokkum, P. G., Franx, M., & Whitaker, K. E. 2015, 798, 115, doi: 10.1088/0004-637X/798/2/115

Li, C., & White, S. D. M. 2009, Monthly Notices of the Royal Astronomical Society, 398, 2177, doi: 10.1111/j.1365-2966.2009.15268.x

Li, Y., Mo, H. J., & Gao, L. 2008, Monthly Notices of the Royal Astronomical Society, 389, 1419, doi: 10.1111/j.1365-2966.2008.13667.x

Lim, S. H., Mo, H. J., Wang, H., & Yang, X. 2016, Monthly Notices of the Royal Astronomical Society, 455, 499, doi: 10.1093/mnras/stv2282

Lu, Y., Wechsler, R. H., Somerville, R. S., et al. 2014, The Astrophysical Journal, 795, 123, doi: 10.1088/0004-637X/795/2/123

Madau, P., & Dickinson, M. 2014, Annual Review of Astronomy and Astrophysics, 52, 415, doi: 10.1146/annurev-astro-081811-125615

Magdis, G. E., Daddi, E., Béthermin, M., et al. 2012, The Astrophysical Journal, 760, 6, doi: 10.1088/0004-637X/760/1/6

Mamon, G. A., Sanchis, T., Salvador-Solé, E., & Solanes, J. M. 2004, Astronomy and Astrophysics, 414, 445, doi: 10.1051/0004-6361:20034155

Mandelbaum, R., Seljak, U., Kauffmann, G., Hirata, C. M., & Brinkmann, J. 2006, Monthly Notices of the Royal Astronomical Society, 368, 715, doi: 10.1111/j.1365-2966.2006.10156.x

Marchesini, D., van Dokkum, P. G., Förster Schreiber, N. M., et al. 2009, The Astrophysical Journal, 701, 1765, doi: 10.1088/0004-637X/701/2/1765

Matthee, J., Schaye, J., Crain, R. A., et al. 2017, Monthly Notices of the Royal Astronomical Society, 465, 2381, doi: 10.1093/mnras/stw2884

Mitra, S., Davé, R., & Finlator, K. 2015, Monthly Notices of the Royal Astronomical Society, 452, 1184, doi: 10.1093/mnras/stv1387

Mitra, S., Davé, R., Simha, V., & Finlator, K. 2017, Monthly Notices of the Royal Astronomical Society, 464, 2766, doi: 10.1093/mnras/stw2527

Moore, B., Lake, G., & Katz, N. 1998, The Astrophysical Journal, 495, 139, doi: 10.1086/305264

More, S., van den Bosch, F. C., Cacciato, M., et al. 2011, Monthly Notices of the Royal Astronomical Society, 410, 210, doi: 10.1111/j.1365-2966.2010.17436.x

Moster, B. P., Naab, T., & White, S. D. M. 2013, Monthly Notices of the Royal Astronomical Society, 428, 3121, doi: 10.1093/mnras/sts261

—. 2017, arXiv:1705.05373 [astro-ph]. https://arxiv.org/abs/1705.05373

Moustakas, J., Coil, A. L., Aird, J., et al. 2013, The Astrophysical Journal, 767, 50, doi: 10.1088/0004-637X/767/1/50

Muzzin, A., Marchesini, D., Stefanon, M., et al. 2013, The Astrophysical Journal, 777, 18, doi: 10.1088/0004-637X/777/1/18

Noeske, K. G., Weiner, B. J., Faber, S. M., et al. 2007, The Astrophysical Journal Letters, 660, L43, doi: 10.1086/517926

Parejko, J. K., Sunayama, T., Padmanabhan, N., et al. 2013, Monthly Notices of the Royal Astronomical Society, 429, 98, doi: 10.1093/mnras/sts314

Patel, S. G., Kelson, D. D., Williams, R. J., et al. 2015, The Astrophysical Journal Letters, 799, L17, doi: 10.1088/2041-8205/799/2/L17

Peng, Y., Maiolino, R., & Cochrane, R. 2015, Nature, 521, 192, doi: 10.1038/nature14439

Peng, Y.-j., Lilly, S. J., Kovač, K., et al. 2010, The Astrophysical Journal, 721, 193, doi: 10.1088/0004-637X/721/1/193

Pillepich, A., Springel, V., Nelson, D., et al. 2018, Monthly Notices of the Royal Astronomical Society, 473, 4077, doi: 10.1093/mnras/stx2656

Reddick, R. M., Wechsler, R. H., Tinker, J. L., & Behroozi, P. S. 2013, The Astrophysical Journal, 771, 30, doi: 10.1088/0004-637X/771/1/30

Rodríguez-Puebla, A., Primack, J. R., Behroozi, P., & Faber, S. M. 2016, Monthly Notices of the Royal Astronomical Society, 455, 2592, doi: 10.1093/mnras/stv2513

Roediger, J. C., & Courteau, S. 2015, Monthly Notices of the Royal Astronomical Society, 452, 3209, doi: 10.1093/mnras/stv1499

Salim, S., Rich, R. M., Charlot, S., et al. 2007, The Astrophysical Journal Supplement Series, 173, 267, doi: 10.1086/519218

Santini, P., Fontana, A., Grazian, A., et al. 2009, Astronomy and Astrophysics, 504, 751, doi: 10.1051/0004-6361/200811434

Schreiber, C., Pannella, M., Elbaz, D., et al. 2015, Astronomy and Astrophysics, 575, A74, doi: 10.1051/0004-6361/201425017

Silk, J., & Mamon, G. A. 2012, Research in Astronomy and Astrophysics, 12, 917, doi: 10.1088/1674-4527/12/8/004

Somerville, R. S., & Davé, R. 2015, Annual Review of Astronomy and Astrophysics, 53, 51, doi: 10.1146/annurev-astro-082812-140951

Somerville, R. S., Gilmore, R. C., Primack, J. R., & Domínguez, A. 2012, Monthly Notices of the Royal Astronomical Society, 423, 1992, doi: 10.1111/j.1365-2966.2012.20490.x

Sparre, M., Hayward, C. C., Feldmann, R., et al. 2017, Monthly Notices of the Royal Astronomical Society, 466, 88, doi: 10.1093/mnras/stw3011

Sparre, M., Hayward, C. C., Springel, V., et al. 2015, Monthly Notices of the Royal Astronomical Society, 447, 3548, doi: 10.1093/mnras/stu2713

Speagle, J. S., Steinhardt, C. L., Capak, P. L., & Silverman, J. D. 2014, The Astrophysical Journal Supplement Series, 214, 15, doi: 10.1088/0067-0049/214/2/15

Sunayama, T., Hearin, A. P., Padmanabhan, N., & Leauthaud, A. 2016, Monthly Notices of the Royal Astronomical Society, 458, 1510, doi: 10.1093/mnras/stw332

Taghizadeh-Popp, M., Fall, S. M., White, R. L., & Szalay, A. S. 2015, The Astrophysical Journal, 801, 14, doi: 10.1088/0004-637X/801/1/14

Taylor, E. N., Franx, M., van Dokkum, P. G., et al. 2009, The Astrophysical Journal, 694, 1171, doi: 10.1088/0004-637X/694/2/1171

Tinker, J., Wetzel, A., & Conroy, C. 2011, ArXiv e-prints, 1107, arXiv:1107.5046

Tinker, J. L., Hahn, C., Mao, Y.-Y., & Wetzel, A. R. 2018a, Monthly Notices of the Royal Astronomical Society, 478, 4487, doi: 10.1093/mnras/sty1263

Tinker, J. L., Hahn, C., Mao, Y.-Y., Wetzel, A. R., & Conroy, C. 2018b, Monthly Notices of the Royal Astronomical Society, 477, 935, doi: 10.1093/mnras/sty666

Tinker, J. L., Leauthaud, A., Bundy, K., et al. 2013, The Astrophysical Journal, 778, 93, doi: 10.1088/0004-637X/778/2/93

Tinker, J. L., Wetzel, A. R., Conroy, C., & Mao, Y.-Y. 2017, Monthly Notices of the Royal Astronomical Society, 472, 2504, doi: 10.1093/mnras/stx2066

Tojeiro, R., Wilkins, S., Heavens, A. F., Panter, B., & Jimenez, R. 2009, The Astrophysical Journal Supplement Series, 185, 1, doi: 10.1088/0067-0049/185/1/1

Tojeiro, R., Eardley, E., Peacock, J. A., et al. 2017, Monthly Notices of the Royal Astronomical Society, 470, 3720, doi: 10.1093/mnras/stx1466

Vale, A., & Ostriker, J. P. 2006, Monthly Notices of the Royal Astronomical Society, 371, 1173, doi: 10.1111/j.1365-2966.2006.10605.x

Velander, M., van Uitert, E., Hoekstra, H., et al. 2014, Monthly Notices of the Royal Astronomical Society, 437, 2111, doi: 10.1093/mnras/stt2013

Vogelsberger, M., Genel, S., Springel, V., et al. 2014, Monthly Notices of the Royal Astronomical Society, 444, 1518, doi: 10.1093/mnras/stu1536

Wang, L., Farrah, D., Oliver, S. J., et al. 2013, Monthly Notices of the Royal Astronomical Society, 431, 648, doi: 10.1093/mnras/stt190

Wang, Y., Yang, X., Mo, H. J., et al. 2008, The Astrophysical Journal, 687, 919, doi: 10.1086/591836

Wechsler, R. H., & Tinker, J. L. 2018, ArXiv e-prints, 1804, arXiv:1804.03097

Wechsler, R. H., Zentner, A. R., Bullock, J. S., Kravtsov, A. V., & Allgood, B. 2006, The Astrophysical Journal, 652, 71, doi: 10.1086/507120

Wetzel, A. R., Cohn, J. D., & White, M. 2009, Monthly Notices of the Royal Astronomical Society, 395, 1376, doi: 10.1111/j.1365-2966.2009.14424.x

Wetzel, A. R., Cohn, J. D., White, M., Holz, D. E., & Warren, M. S. 2007, The Astrophysical Journal, 656, 139, doi: 10.1086/510444

Wetzel, A. R., Tinker, J. L., & Conroy, C. 2012, Monthly Notices of the Royal Astronomical Society, 424, 232, doi: 10.1111/j.1365-2966.2012.21188.x

Wetzel, A. R., Tinker, J. L., Conroy, C., & van den Bosch, F. C. 2013, Monthly Notices of the Royal Astronomical Society, 432, 336, doi: 10.1093/mnras/stt469

—. 2014, Monthly Notices of the Royal Astronomical Society, 439, 2687, doi: 10.1093/mnras/stu122

Wetzel, A. R., & White, M. 2010, Monthly Notices of the Royal Astronomical Society, 403, 1072, doi: 10.1111/j.1365-2966.2009.16191.x

Weyant, A., Schafer, C., & Wood-Vasey, W. M. 2013, The Astrophysical Journal, 764, 116, doi: 10.1088/0004-637X/764/2/116

Whitaker, K. E., van Dokkum, P. G., Brammer, G., & Franx, M. 2012, The Astrophysical Journal Letters, 754, L29, doi: 10.1088/2041-8205/754/2/L29

White, M. 2002, The Astrophysical Journal Supplement Series, 143, 241, doi: 10.1086/342752

White, M., Cohn, J. D., & Smit, R. 2010, Monthly Notices of the Royal Astronomical Society, 408, 1818, doi: 10.1111/j.1365-2966.2010.17248.x

Wilkinson, D. M., Maraston, C., Goddard, D., Thomas, D., & Parikh, T. 2017, arXiv:1711.00865 [astro-ph]. https://arxiv.org/abs/1711.00865

Yang, X., Mo, H. J., & van den Bosch, F. C. 2006, The Astrophysical Journal Letters, 638, L55, doi: 10.1086/501069

—. 2009, The Astrophysical Journal, 695, 900, doi: 10.1088/0004-637X/695/2/900

Yang, X., Mo, H. J., van den Bosch, F. C., & Jing, Y. P. 2005, Monthly Notices of the Royal Astronomical Society, 356, 1293, doi: 10.1111/j.1365-2966.2005.08560.x

York, D. G., Adelman, J., Anderson, Jr., J. E., et al. 2000, The Astronomical Journal, 120, 1579, doi: 10.1086/301513

Zehavi, I., Contreras, S., Padilla, N., et al. 2018, The Astrophysical Journal, 853, 84, doi: 10.3847/1538-4357/aaa54a

Zehavi, I., Zheng, Z., Weinberg, D. H., et al. 2011, The Astrophysical Journal, 736, 59, doi: 10.1088/0004-637X/736/1/59

Zheng, Z., Coil, A. L., & Zehavi, I. 2007, The Astrophysical Journal, 667, 760, doi: 10.1086/521074

Zu, Y., & Mandelbaum, R. 2015, Monthly Notices of the Royal Astronomical Society, 454, 1161, doi: 10.1093/mnras/stv2062